Afdelingen for Bærende Konstruktioner
Department of Structural Engineering
Danmarks Tekniske Højskole · Technical University of Denmark

A Constitutive Model for Normal and High Strength Concrete

Kaare K. B. Dahl

Serie R No 287 1992

Summary

The Calibration and Use of a Triaxial Cell

This report describes in detail the equipment and techniques used for testing concrete in a triaxial cell. In a triaxial cell it is possible to induce a well defined triaxial stress field in a cylindrical test specimen. Not all possible combinations of stress fields can be generated in a triaxial cell, only stress fields where two of the three principal stresses are equal.

The subjects described in this report are the observations and conclusions, concerning the test equipment, of a major research program aimed at testing concrete under triaxial stresses. The major problems encountered were primarily how to generate a well defined triaxial stress field in a concrete cylinder, with the minor principal stresses in the range 0 to 140 MPa, and secondly how to measure the concrete strains at the same range of stresses.

The report pays particular attention to the following subjects:

1/ Describing the equipment needed for testing.
2/ Calibration of the test equipment.
3/ Preparing test specimens.
4/ Describing the adopted testing procedure.

A Failure Criterion for Normal and High Strength Concrete

This report deals with the strength of concrete subjected to stresses in more than one direction. The report describes a large test program aimed at determining a failure criterion for concrete, including high strength concrete. The concretes investigated were ordinary concretes with a varying uniaxial strength between 10 and 110 MPa.

A total of 240 test specimens were tested with the minor principal stress ranging between 0 and 140 MPa. All tests were conducted with all principal stresses compressive and the two minor principal stresses being equal. The tests were performed using a triaxial cell. The construction and use of this cell is described in detail in ***The Calibration and Use of a Triaxial Cell.***

The test results showed a large difference between the ultimate strength of low and normal strength concretes, especially for high relative stress loadings. The difference in ultimate strength of normal and high strength concrete was not large but still noticeable. The test results showed also a drastic change in the failure envelope when testing mortars and pastes, as compared to ordinary concrete.

The test results are compared to the Ottosen model, and the Mohr-Coulomb model. Both models are changed in order for them to reflect the new knowledge found in this investigation.

A Constitutive Model for Normal and High Strength Concrete

This report deals with the deformations of concrete subjected to stresses in more than one direction. The report describes a large test program aimed at determining a constitutive model for concrete, including high strength concrete. The concretes investigated were ordinary concretes with a varying concrete strength between 10 and 110 MPa.

The experimental investigation is an integral part of an investigation into the strength of concrete under multiaxial stresses as reported in ***A Failure Criterion for Normal and High Strength Concrete.*** In this investigation a total of 240 test specimens were tested with the minor principal stress ranging between 0 and 140 MPa. Of these 240 test specimens 91 were tested with strain gauges mounted. All the tests were conducted with the principal stresses compressive and the two minor principal stresses being equal. The tests were performed using a triaxial cell. The construction and use of this cell is described in detail in ***The Calibration and Use of a Triaxial Cell.***

The test results showed a surprisingly plastic behavior of the concretes under triaxial stresses. In the case of low strength concretes, deformations of more than 20% were experienced, and in the case of very high strength concretes, deformations of more than 8% were experienced.

Based on these test results an improvement of the Ottosen constitutive model is presented. The model is based on the non-linear elastic theory and is very simple and easy to use. The model has also been compared to experimental results from other investigations. Although widely different concrete strengths, test rigs, and load paths have been used in these investigations, it has been found that the model predicts the deformational behavior of concrete well within acceptable limits.

Resumé

The Calibration and Use of a Triaxial Cell

Denne rapport indeholder en detaljeret beskrivelse af det udstyr, og de teknikker der behøves for at kunne prøve beton i en triaxial celle. I en triaxial celle er det muligt at udsætte en beton cylinder for en forud fastlagt tre-akset spændingstilstand. Det er dog ikke muligt i en sådan celle, at frembringe en hvilken som helst tre-akset spændingstilstand, idet cellens opbygning gør, at to af de tre hovedspændinger altid vil være lige store.

I denne rapport er beskrevet de observationer og de konklusioner vedrørende forsøgsopstillingen, der er fremkommet under et større forskningsprogram rettet mod betons styrke og tøjningsforhold under tre-aksede spændingstilstande. De største problemer der opstod var, dels at kunne sikre en forud fastlagt spændingstilstand, hvor de mindste hovedspændinger var i området 0 til 140 MPa, og dels at kunne måle de tilsvarende tøjninger i betonen.

Rapporten beskriver indgående følgende emner:

1/ Beskrivelse af forsøgsopstillingen.
2/ Kalibrering af udstyret i forsøgsopstillingen.
3/ Den nødvendige forberedelse af prøvelegemer.
4/ Proceduren for den egentlige prøvning.

A Failure Criterion for Normal and High Strength Concrete

Denne rapport omhandler betons styrke, når denne er udsat for spændinger i mere end én retning. Rapporten beskriver et stort forsøgsprogram rettet mod at bestemme et brudkriterium for beton, inklusiv højstyrkebeton. De anvendte beton var normale betoner, med en én-akset styrke på mellem 10 og 110 MPa.

I alt blev 240 prøvelegemer afprøvet med den mindste hovedspænding varierende mellem 0 og 140 MPa. Alle forsøgene blev udført med trykspændinger overalt, og med de to mindste hovedspændinger lige store. Forsøgene blev udført i en triaxial celle. Opbygningen og brugen af denne celle er udførligt beskrevet i ***The Calibration and Use of a Triaxial Cell.***

Forsøgsresultaterne viste en afgørende forskel i den tre-aksede styrke for lavstyrke beton contra normalstyrke beton, specielt når de mindste hovedspænding steg i styrke. Forskellen mellem normal og højstyrke betoner viste sig ikke at være særligt stor, men dog ikke uden betydning. Sammenlignende forsøg med beton, mørtel og cement pasta viste, at der sker en drastisk forandring i brudfladens udseende når indholdet af det grove tilslag mindskes.

Forsøgsresultaterne er slutteligt sammenlignet med Ottosens brudkriterium, samt Mohr-Coulomb brudkriteriet. Begge brudkriterier er foreslået ændret, således at de nu reflekterer den nye viden fremkommet i dette projekt.

A Constitutive Model for Normal and High Strength Concrete

Denne rapport omhandler betons deformationer, når denne er udsat for spændinger i mere end én retning. Rapporten beskriver et stort forsøgsprogram rettet mod at bestemme en konstitutiv model for beton, inklusiv højstyrkebeton. De anvendte beton var normale betoner, med en én-akset styrke på mellem 10 og 110 MPa.

De, i denne rapport beskrevne forsøg, er en integreret del af en undersøgelse af betons styrke under fleraksede påvirkninger, som rapporteret i ***A Failure Criterion for Normal and High Strength Concrete***. I denne undersøgelse blev i alt 240 prøvelegemer afprøvet med den mindste hovedspænding varierende mellem 0 og 140 MPa. Af disse 240 prøvelegemer var 91 bestykket med strain gauges for at måle deformationerne. Alle forsøgene blev udført med trykspændinger overalt, og med de to mindste hovedspændinger lige store. Forsøgene blev udført i en triaxial celle. Opbygningen og brugen af denne celle er udførligt beskrevet i ***The Calibration and Use of a Triaxial Cell.***

Forsøgsresultaterne viste en overraskende plasticitet hos beton udsat for treaksede belastninger. Således blev der for lavstyrke beton målt deformationer over 20%, og for højstyrke beton målt deformationer over 8%.

På baggrund af resultaterne fra forsøgene er der foreslået en forbedring af Ottosens konstitutive model. Modellen er baseret på den ikke-lineære elasticitetsteori og er simpel i sin opbygning, samt nem at anvende. Modellen er også blevet sammenlignet med andre publicerede forsøgsresultater. Selvom der i disse undersøgelser er blevet benyttet meget forskellige betoner, forsøgsopstillinger samt belastningmåder, er det konstateret, at modellen forudsiger betons deformationer med meget begrænsede afvigelser.

List of contents

Notation 1

1 Introduction 3

2 Experimental program 5
2.1 The scope of the experimental program 5
2.2 Description of the concretes 6
2.3 Strain gauges 9

3 The proposed constitutive model 11
3.1 Characteristics of concrete deformational behavior 11
3.2 Description of the proposed constitutive model 12
3.2.1 The hydrostatic stress-strain curve 13
3.2.2 The non-linearity index 15
3.2.3 The initial deviatoric Young's modulus 16
3.2.4 The secant value of Young's modulus 18
3.2.5 The apparent Poisson's ratio 20
3.3 Summary 25

4 Evaluation of the proposed model 27
4.1 Comparison between the model and triaxial test results . . 27
4.2 Comparison with other triaxial investigations 31
4.2.1 Hobbs [74.1] 31
4.2.2 Ferrara et.al. [76.1] 33
4.2.3 Bellotti and Ronzoni [84.1] 34
4.2.4 Newman and Newman [72.1] 34
4.2.5 Stöckl and Grasser [76.2] 35
4.2.6 van Mier [84.3] 37
4.3 Comparisons with biaxial investigations 41
4.3.1 Kupfer [73.1], normal strength concrete 41
4.3.2 Kupfer [73.1], high strength concrete 43
4.4 Summary of verification 44

5 Concrete versus mortar 47

6 Conclusion 51

References 53

Appendix 1 Strain diagrams

Appendix 2 Experimental results

Notation

In this report standardized SI units and European symbols have been used. Any deviations from this are described in the text when they occur. Furthermore will the convention that tension is assumed positive be used throughout the report. As a consequence, $0>\sigma_1>\sigma_2>\sigma_3$ corresponds to a stress state where all stresses are compressive.

D	Parameter in equation for uniaxial stress-strain curve
E_0	Initial Young's modulus in uniaxial compression
E_i	Deviatoric initial Young's modulus
E_c	Peak secant value of Young's modulus in uniaxial compression, $E_c=f_c/(-\epsilon_c)$
E_f	Peak secant value of Young's modulus in general form, $E_f=(\sigma_{3f}-\sigma_{0,max})/(\epsilon_{3f}-\epsilon_{0,max})$
E_s	Secant value of Young's modulus
f_c	Uniaxial compressive strength of concrete ($f_c>0$)
I_1, I_2, I_3	Invariants of the stress tensor
J_1, J_2, J_3	Invariants of the deviatoric stress tensor
β	Non-linearity index
β_l	Linearity limit for the apparent Poisson's ratio
ϵ_c	Strain at peak stress in uniaxial compression ($\epsilon_c<0$)
ϵ_0	Hydrostatic strain, $\epsilon_3=\epsilon_2=\epsilon_1$
$\epsilon_{0,max}$	Maximum level of hydrostatic strain encountered
ϵ_1,ϵ_2,ϵ_3	Principal strains (extension positive)
ϵ_{1f}	Major principal strain at failure
ϵ_{3f}	Minor principal strain at failure
ν	Poisson's ratio
ν^a	Apparent Poisson's ratio
ν_i^a	Initial value of the apparent Poisson's ratio
ν_f^a	Value of apparent Poisson's ratio at failure
σ_0	Hydrostatic stress ($\sigma_1=\sigma_2=\sigma_3$)
$\sigma_{0,max}$	Maximum level of hydrostatic stress encountered
σ_1, σ_2, σ_3	Principal stresses (tension positive)
σ_{1f}	Major principal stress at failure
σ_{3f}	Minor principal stress at failure

Chapter 1

Introduction

Determining the deformations of concrete subjected to any type of loading is a very complex thing. Due to concretes inherent heterogeneity numerous factors affect the deformations. Among these factors a few can be mentioned here: The type of aggregate, the size and size distribution of the aggregate, and the number and distribution of pores and voids. These factors are only some of the internal factors that can affect the deformations. Besides these internal factors uncountable external factors may influence the deformations of concrete.

The complexity of concrete makes it very hard to establish a correct constitutive model. It is symptomatic that although quite a lot of research has been channeled into concrete research the last 100 years a conclusion has yet to be reached regarding the size of a simple parameter such as the strain at peak stress in the uniaxial compression test.

Especially the last couple of decades have seen a growing interest, and an increasing research, into developing a model that can describe the deformational behavior of concrete within acceptable limits. This interest has been due to the spreading use of computers in designing concrete structures, and the development of more and more versatile computer programs.

In trying to establish a constitutive model many widely different paths have been taken. These paths are ranging from the very simple early models developed by curve fitting, to the elastic-plastic-fracturing model by Bazânt and Kim [79.2]. The models of the former type tend to be applicable only to a very narrow band of concretes, whereas the latter tend to yield very good results for most types of loadings and unloadings, but they are hard to calibrate to the specific concrete in question.

Also the last 2 decades have seen a growing interest and use of high strength, high performance concretes. Although these new concretes are made of the same raw materials they in many cases show a very different behavior from the older normal strength concretes. There is therefore a very pressing need for investigating the deformational behavior of these new concretes because they in many ways represent a new material.

Due to the very complex behavior there is a need for simplicity in any constitutive modelling of concrete. In this report it has therefore been attempted to establish a constitutive model that is simple, and yet applicable to normal type concretes ranging in strength from 10 to 100 MPa. The simplicity has been achieved by using the non-linear elastic theory, and by limiting the model to cover only short-term compressive loadings.

Chapter 2

Experimental program

In this chapter a more detailed description of the test program will be given. Also described are the test equipment and the concretes used in this investigation.

2.1 The scope of the experimental program

The main purpose of this investigation has been to establish triaxial stress-strain curves for normal and high strength concrete, and to investigate the influence of the uniaxial concrete strength on these stress-strain curves. Furthermore was the end result of the investigation to produce a constitutive model for the deformational response of concrete which covered concretes with an uniaxial strength up to 100 MPa.

In order to investigate the deformational behavior of concrete under triaxial loadings, a triaxial cell was used. This cell, and its calibration and use, has been extensively described by the author in [92.1]. Therefore no attempt will be made, in this report, to describe the cell or the use of it.

The relation between the uniaxial strength and the deformational behavior of concrete was investigated by testing 7 different concrete mixes. The concretes were designed to have an uniaxial compressive strength of 10, 35, 50, 70, 85, 100, and 110 MPa. The concretes are named 'Bnnn-m' where 'nnn' is the uniaxial strength level, and 'm' is the batch number. The concretes were designed to be like ordinary concretes, that is, the binder content was kept low, and the aggregate content kept high.

Each concrete was tested with the major principal stress ranging from 0 to 140 MPa. In order to compare concretes with different strengths, the test program planned for the concretes to be tested with the major principal stress as follows:

$-0 \cdot f_c < \sigma_1 = \sigma_2 \leq -2 \cdot f_c$: $-\sigma_1/f_c$ = 0.2, 0.4, 0.6, 0.8, 1.0, 1.2, 1.4, 1.6, 1.8, 2.0

$-2 \cdot f_c < \sigma_1 = \sigma_2 \leq -4 \cdot f_c$: $-\sigma_1/f_c$ = 2.5, 3.0, 3.5, 4.0

$-4 \cdot f_c < \sigma_1 = \sigma_2 \leq -6 \cdot f_c$: $-\sigma_1/f_c$ = 5.0, 6.0

$-6 \cdot f_c < \sigma_1 = \sigma_2 \leq -14 \cdot f_c$: $-\sigma_1/f_c$ = 8.0, 10.0, 14.0

The different concretes were tested as far as the capacity of the test equipment allowed, i.e. B100 was tested with the major principal stresses up to 140 MPa, that is $-\sigma_1/f_c = 1.4$.

In all the tests, the major and the intermediate principal stresses were equal. This means that the results of the test program lie exclusively on the compression meridian. This limitation is due to the limitations of the triaxial cell, as described in [92.1].

All the test specimens were tested using a 'normal' load path, that is loading along the hydrostatic axis, until a predetermined stress level is reached, hereafter increasing the deviator stress until failure.

The load speed was the same for all the tests, and was equal to 0.3 MPa/s.

In order to investigate the influence of the aggregate size, and -content, 2 mortars, and 1 paste were cast. The mix design for these paste and mortars was determined simply by removing one or more of the three aggregate types in the mix design for B070. Hereby it was ensured that the uniaxial strength of the mortars and the paste was approximately the same as the uniaxial strength of B070.

The mix design for mortar B, M070B, was established by removing all of the crushed granite from the mix design of B070. The mix design for mortar A, M070A, was established by removing all of the Gravelit from the mix design of M070B. Finally the mix design for the paste, P070, was established by removing all of the sand from the mix design of M070A.

2.2 Description of the concretes

The investigation of the deformational behavior was undertaken parallel to an investigation of the triaxial strength of concrete. Approximately a third of the specimens used in the latter investigation was tested with strain gauges mounted. The deformation measurements from these specimens are the ones described in this report.

The results of the triaxial strength investigation are described in [92.2]. Also in [92.2] are

the materials, the concretes, and the curing conditions extensively described. As a consequence only the mix proportions and the uniaxial strength results of the concretes will be included in this report. The numbers of the concretes and the batches used in this report are therefore referring to the concretes described in [92.2], i.e. concrete B010-3 in this report is identical to the concrete B010-3 described in [92.2].

A total of 7 concretes, 2 mortars, and 1 cement paste, were used in the investigation. The mix proportions of the individual concretes are given in table 2.1, and the uniaxial compressive strengths of the mixes are given in table 2.2.

Concrete / Material	B010 3	B035 3	B050 3	B070 2	B085 3	B100 3	B110 2	P070	M070 A	M070 B
Cement (*)	129	247	260	309	320	375	390	1030	598	462
Fly ash	69	100	40	-	45	-	-	-	-	-
MS-slurry	-	-	36	55	60	75	76	183	106	82
Water	170	170	150	129	95	70	63	430	249	192
Sand (0-4 mm)	754	618	600	598	610	615	521	-	1157	904
Gravelit (4-8 mm)	246	244	257	265	186	188	247	-	-	395
Granite (4-16 mm)	985	977	1026	1061	1106	1120	989	-	-	-
Conplast 212	-	-	1.4	2.0	2.0	2.3	2.4	-	-	-
Peramin F	-	-	-	3.1	6.3	8.3	8.6	-	-	-

Table 2.1: Mix proportions for the different concretes, mortars, and paste, used in the investigation. All units are kg/m^3.

(*): The cement used was, B085: low-alkali cement, B100: white cement, the remaining: rapid hardening cement.

For each concrete 6 Ø100·200 mm cylinders were tested in order to determine the uniaxial compressive strength of that particular concrete, which in the investigation was varied between 10 and 110 MPa. All the cylinders were tested in a 200 tons MP MFL compression

jack controlled by a Walter+Bai servo controller.

All of the test cylinders were ground accurately plane by means of a diamond cutting spindle. In the uniaxial compression tests, wood fiber plates were used between the steel loading plates and the concrete. Previous studies at the Department of Structural Engineering have shown these fiber plates to have no influence on the strength measurements. The cylinders were tested at a rate of 0.7 MPa/s, as specified by the Danish National Code [84.2].

	Strength results	
	f_c (MPa)	s.dev. (%)
B010	17.08	5.74
B035	40.41	3.54
B050	51.54	6.34
B070	71.65	2.23
B085	88.39	4.41
B100	99.82	2.95
B110	108.76	3.83
P070 (*)	30.42	14.88
M070-A	73.49	1.88
M070-B	69.61	3.33

Table 2.2: Uniaxial compressive strength of the concretes, mortars, and the paste. The compressive strengths are the average result of 6 test cylinders Ø100·200 mm.

(*) The paste cylinders failed due to the very severe shrinkage cracks that appeared shortly after the cylinders were removed from the water storage. The compressive strength shown here is therefore not the uniaxial compressive strength of the cement paste itself, but that of the shrink-cracked cement paste.

2.3 Strain gauges

On each of the cylinders a total of 4 strain gauges were mounted. 2 strain gauges were used for measuring the vertical deformation, and 2 strain gauges were used for measuring the horizontal deformation. The gauges were mounted diametrically opposing each other, and placed at mid height of the test specimen.

In order to minimize the influence of excentrical loading, difference in placement etc. the mean value of the signals from the two opposing strain gauges have been used for determining the deformations of the concrete. In some of the tests only one of the two strain gauges remained intact throughout the entire test. In these cases only the unbroken strain gauge has been used for determining the deformations in that particular direction. This procedure has not been found to inflict any significant error in determining the concrete strains. This because a close inspection of all of the test results revealed that the two opposing gauge signals on each of the specimens did not deviate in any significant way.

The strain gauges used were a foil-type post-yield strain gauge, 60 mm long. The strain gauge itself, and the calibration of the strain gauge are extensively described in [92.1].

Chapter 3

The proposed constitutive model

Formulation of a constitutive model to describe the deformational behavior of concrete subjected to any type of loading has proven to be very difficult. Over the years many researchers have proposed different constitutive models based on many different theories. Some of the more important ones are described by Kim in [91.1].

In this report, a proposal for an improvement of the Ottosen constitutive model for short-time loadings [79.1] is made, and in this chapter the model is defined and described. However, prior to defining a model it is necessary to summarize some of the characteristics of concrete deformational behavior.

3.1 Characteristics of concrete deformational behavior

When studying the deformational behavior of concrete, certain characteristics appear.

1/ The stress-strain curve of concrete subjected to hydrostatic stress, is not linear as one would expect. For high hydrostatic stresses the stress-strain curve displays both a softening and a stiffening behavior.

2/ The stress-strain curve is depending on all three stress invariants.

3/ When approaching failure, concrete exhibits an increase in volume, the so-called dilatation.

4/ The initial deviatoric Young's modulus, E_i, is depending on the prior loading history.

5/ The secant value of Young's modulus, E_s, is depending on, among other things, the type of loading, and the type of concrete.

It therefore follows that any constitutive model must answer to all, or most of, these characteristics.

3.2 Description of the proposed constitutive model

The proposed model is based of the non-linear elasticity, and is an extension of the original proposed model of Ottosen [79.1]. The Ottosen model has later been adopted by CEB to be included in the CEB Model Code 1990 [90.1].

The new revised model responds well to the above mentioned characteristics of the general stress-strain curve for concrete in that:

1/ Dilatation is included.
2/ All three stress invariants are included.
3/ Smooth stress-strain curves are obtained.
4/ The hydrostatic stress-strain curve is included.
5/ The ultimate strength of concrete is realistic.
6/ High strength concrete up to 100 MPa is included.
7/ Uniaxial, biaxial, and triaxial stress-strain curves are obtained.

Furthermore is the model very simple to use, and calibration is performed using only data readily obtained by the standard uniaxial compression test.

Construction of the model is carried out in 5 steps:

1/ Determination of the hydrostatic stress-strain curve.
2/ Determination of the non-linearity index.
3/ Determination of the Young's modulus for initial deviatoric loading.
4/ Changing the secant value of Young's modulus.
5/ Determination of the apparent value of Poisson's ratio.

In the present form the model is only intended for compressive stress states where the principal stresses are ever increasing or kept constant. Unloading and cyclic loadings are therefore beyond the capabilities of the model. Likewise is tension not considered. It is, however, relatively easy to extend the model also to include tensile stresses as shown in [79.1]. At present, however, the model does not consider tensile loadings.

Furthermore is the model only valid for stress up to peak value. Although the post peak

behavior is important, the model has not been extended to include this. One reason is the general lack of experimental evidence of the post peak behavior of concrete under multiaxial stress states. However, as will be shown later it is very easy to expand the model in order to be able to simulate different post peak behaviors.

In the following the model will be constructed. In order to describe the stress-strain curves, a number of symbols are used. These symbols are defined in the text when they occur, and furthermore are the definition of most of these symbols shown in Fig. 3.1.

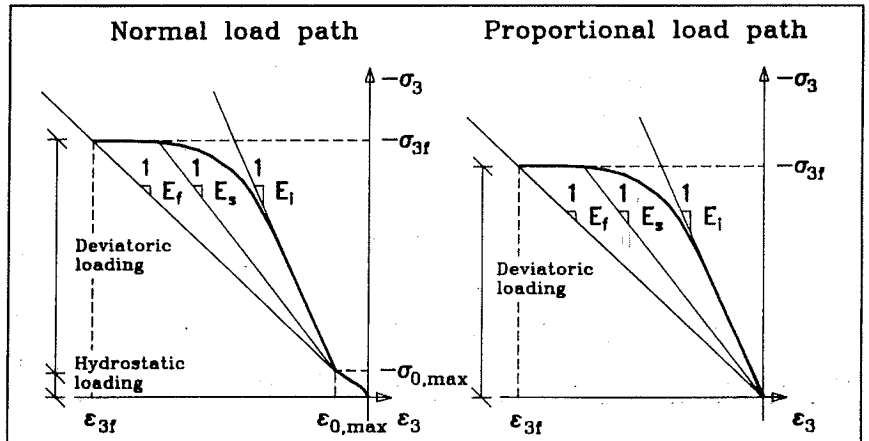

Fig. 3.1: Symbols used in the model.

3.2.1 The hydrostatic stress-strain curve

Contrary to the general belief concrete exhibits nonlinear deformational response to pure hydrostatic loading. The initial response is a compaction of the concrete followed by an expansion for increasing hydrostatic stresses.

Experimental results from Kotsovos & Newman [78.1], show that the change between compaction and expansion occurs for $-\sigma_0/f_c \approx 2$. This is confirmed by Chen [82.1], and also indicated by the results reported in this investigation.

It was found that a sufficiently accurate expression for the hydrostatical stress-strain curve is as given in (3.1).

$$\epsilon_0 = \frac{\left(-\frac{\sigma_0}{f_c}\right)^{2.25}}{2000} - \frac{\left(-\frac{\sigma_0}{f_c}\right)^{1.80}}{600} \qquad (3.1)$$

The test results of this investigation are shown along with eq. (3.1) in Fig. 3.2 and 3.3.

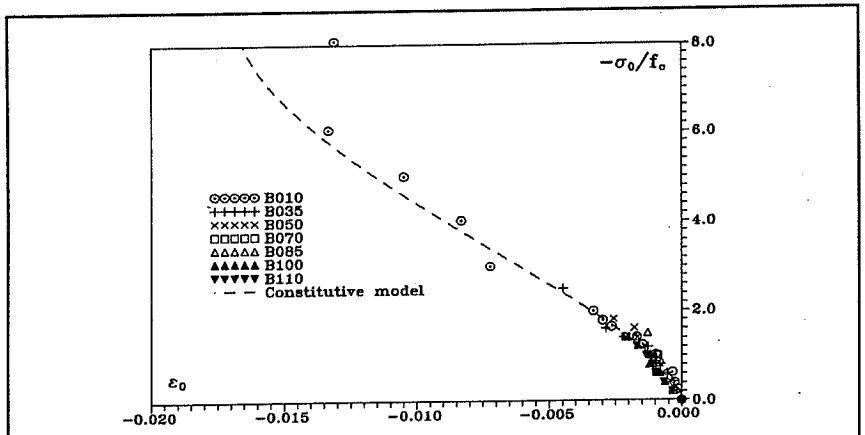

Fig. 3.2: Hydrostatic part of constitutive model compared to test data.

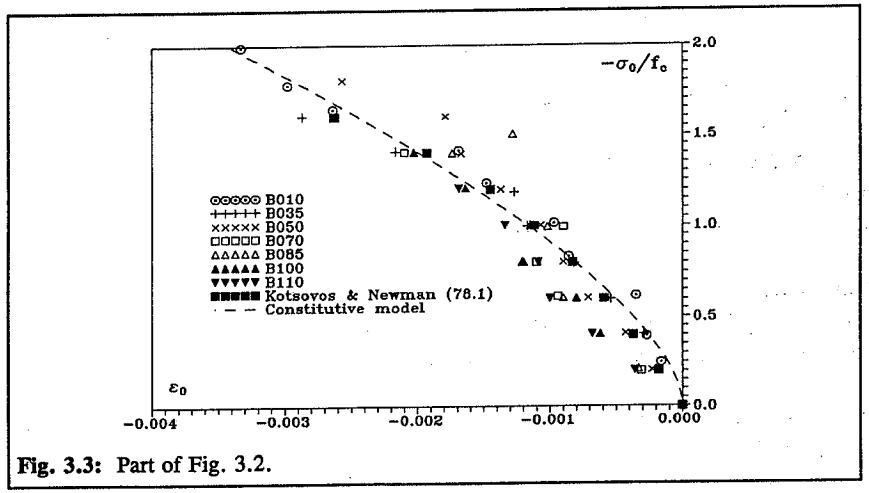

Fig. 3.3: Part of Fig. 3.2.

Also shown in Fig. 3.3 are the test results of Kotsovos and Newman [78.1], and it is seen that these test results and the model correspond well to each other. It is seen in Fig. 3.3 that the hydrostatic stress-strain curve is depending on the uniaxial compressive strength, or more likely the initial value of Young's modulus, E_0. However, in order to simplify the model, and because the hydrostatic strains are very small compared to the deviatoric strains, the dependency of the hydrostatic stress-strain curve with respect to the specific concrete has been left to later refinements.

Lastly in Fig. 3.4 is the model shown compared to the major principal strains of concrete B010-3.

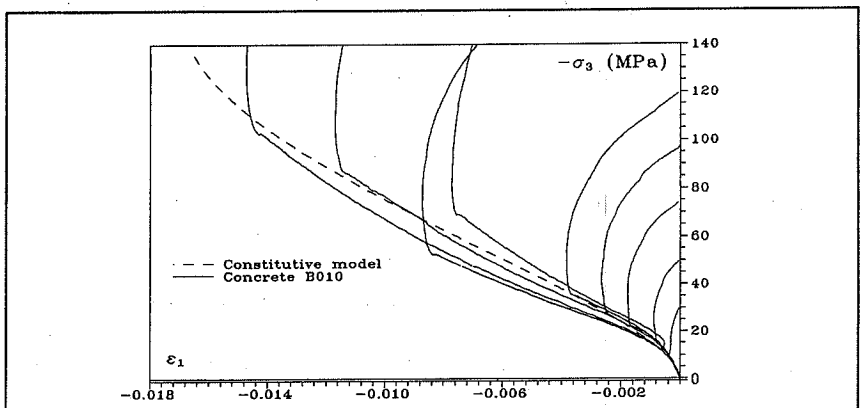

Fig. 3.4: Hydrostatic stress-strain model compared to test results from concrete B010-3

It is clearly seen that the proposed model possesses all the characteristics of the hydrostatic stress-strain curve, and that it compares well to the test results.

3.2.2 The non-linearity index

Prior to describing the constitutive model it is necessary to define the non-linearity index β. β is defined as a measure of the actual stress state in relation to the intended failure stress. As described earlier the model is only valid for increasing compressive loads. It is generally accepted that a pure hydrostatic stress state ($\sigma_3=\sigma_2=\sigma_1$) does not lead to failure no matter how high the hydrostatic stress level is. In determining the non-linearity index the part of the load path with only pure hydrostatic stresses is therefore disregarded.

A convenient measure for the actual loading is therefore $\sigma_3 - \sigma_{0,max}$ where σ_3 is the minor principal stress, and $\sigma_{0,max}$ is the maximum previously encountered pure hydrostatic stress. Similar to the measure for the actual loading, is the measure for the failure stress defined as $\sigma_{3f} - \sigma_{0,max}$ where σ_{3f} is the minor principal stress at failure. β is then defined as given in eq. (3.2).

$$\beta = \frac{\sigma_3 - \sigma_{0,max}}{\sigma_{3f} - \sigma_{0,max}} \tag{3.2}$$

By defining β this way, β can be considered an effective deviatoric stress, and $\beta<1$, $\beta=1$, and $\beta>1$ then correspond to stress states located inside, on, and outside the failure surface.

The failure stress, σ_{3f}, is determined by using a suitable failure criterion. In this report the failure criterion of the author will be used exclusively. This failure criterion is described in detail in [92.2]. One of the advantages of using this failure criterion is that the failure state is a function of all three stress invariants. Hereby the resulting stress-strain curve will also be a function of all three stress invariants.

It must be emphasized that any failure criterion can be used. This because the failure criterion is used only in determining the failure stresses. The failure stresses are in turn mainly used in determining the non-linearity index, and thus will not influence the shape of the stress-strain curve. The failure stresses are also used in determining the secant value of Young's modulus at failure. However, using different failure criterions will not have a large influence on the secant modulus at failure since the prediction of the failure stresses does not vary much in the different failure criterions. Using other failure criterions than the one proposed in [92.2] will therefore only influence to a lesser degree the strain at peak stress, not the shape of the stress-strain curve.

3.2.3 The initial deviatoric Young's modulus

The initial deviatoric Young's modulus, E_i, is defined as the initial slope of the stress-strain curve (minor principal stress and strain) for loadings other than hydrostatic loads, see also Fig. 3.1.

As previously described the hydrostatic stress-strain curve is not linear. This is due to damage occurring in the concrete when subjected to hydrostatic loads. Chinn and Zimmerman [65.1] have reported loss of uniaxial strengths up to 40% after high hydrostatic loadings. A consequence of this is that the initial slope of the deviatoric stress-strain curve will diminish the higher hydrostatic loads the concrete has been subjected to. This can also be observed in

the test results here presented. The results show that the drop in E_i is high for small hydrostatic loads, and flattens out for increasing hydrostatic loads. Also seen is that the drop in E_i is relatively higher for the low strength concretes, as compared to the higher strength concretes.

The test results indicates, for the range of concretes and the range of hydrostatic loads used in this investigation, that the value of E_i approaches a constant value. This constant value is depending on the concrete tested, and it has been found that E_c is a good measure for this constant value.

An equation that describes this behavior must also include that in the case of uniaxial tests, biaxial tests, and triaxial tests using proportional load paths, E_i equals that of E_0. An equation that displays all of the above mentioned characteristics, along with having the correct border conditions has been found to be as given in eq. (3.3)

$$E_i = E_c + \frac{E_0 - E_c}{-\frac{\sigma_{0,max}}{f_c} \cdot \frac{E_0}{E_c} + 1} \tag{3.3}$$

This equation, along with the test results is shown in Fig. 3.5.

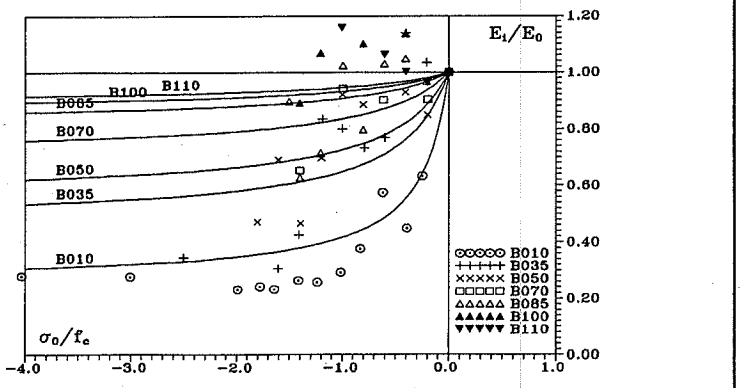

Fig. 3.5: Measured initial value of the deviatoric Young's modulus compared to eq. (3.3).

It is seen that there is some scatter in the test results. This is most probably due to the lack of accuracy when measuring very small strains. However eq. (3.3) seems to yield a good

estimate of the initial deviatoric Young's modulus.

3.2.4 The secant value of Young's modulus

Consider first the uniaxial stress-strain curve. According to the CEB Model Code 1990 [90.1], the uniaxial stress-strain curve can be approximated by eq. (3.4).

$$-\frac{\sigma}{f_c} = \frac{\frac{E_0}{E_c}\cdot\frac{\epsilon}{\epsilon_c} - \left(\frac{\epsilon}{\epsilon_c}\right)^2}{1 + \left(\frac{E_0}{E_c} - 2\right)\frac{\epsilon}{\epsilon_c}} \tag{3.4}$$

This equation has been shown to correspond very well to experimental results, i.e. in [92.3]. The original form of eq. (3.4) is given in eq. (3.5).

$$-\frac{\sigma}{f_c} = \frac{\frac{E_0}{E_c}\cdot\frac{\epsilon}{\epsilon_c} + (D-1)\left(\frac{\epsilon}{\epsilon_c}\right)^2}{1 + \left(\frac{E_0}{E_c} - 2\right)\frac{\epsilon}{\epsilon_c} + D\left(\frac{\epsilon}{\epsilon_c}\right)^2} \tag{3.5}$$

The difference between the two equations lies in the parameter D. The parameter D is mostly used for controlling the descending part of the stress strain curve, and has very little effect on the ascending part. In the CEB Model Code 1990 [90.1] the parameter D has been chosen to 0.

In this report it has been chosen to limit the applicability of the model to stresses up to and including the peak value. This has been decided because the knowledge of the descending part of the stress-strain curve in triaxial tests is very limited. Furthermore, since eq. (3.4) has been shown to correspond well to the uniaxial compression stress-strain curve, the parameter D will also in this model be equal to 0. However, using eq. (3.5) rather than (3.4) in the subsequent calculations offers the possibility of simulating different post-peak behaviors by changing the value of D.

Using only simple algebra it is possible to solve eq. (3.4) with respect to the secant value, E_s, of Young's modulus. The resulting equation for E_s is given in eq. (3.6).

$$E_s = \tfrac{1}{2}E_0 + \frac{\sigma}{f_c}\left(\tfrac{1}{2}E_0 - E_c\right) \pm \sqrt{\left[\tfrac{1}{2}E_0 + \frac{\sigma}{f_c}\left(\tfrac{1}{2}E_0 - E_c\right)\right]^2 + \frac{\sigma}{f_c}E_c^2} \tag{3.6}$$

In the equation the positive and the negative sign refers to the ascending and the descending part of the stress-strain curve, respectively.

It is now possible to generalize eq. (3.6) to include the biaxial and triaxial cases by substituting the following parameters:

- the initial Young's modulus, E_0, with the initial deviatoric Young's modulus, E_i
- the uniaxial secant value of Young's modulus at failure, E_c, with the secant value of Young's modulus at failure under generalized loadings, E_f
- the uniaxial stress ratio ($-\sigma/f_c$) with the non-linearity index, β

Eq. (3.6) then becomes that of eq. (3.7).

$$E_s = \tfrac{1}{2}E_i - \beta\left(\tfrac{1}{2}E_i - E_f\right) \pm \sqrt{\left[\tfrac{1}{2}E_i - \beta\left(\tfrac{1}{2}E_i - E_f\right)\right]^2 - \beta E_f^2} \tag{3.7}$$

Left now is to determine the secant value of Young's modulus at failure under generalized loadings, E_f. E_f is defined in the same way as the non-linearity index, that is, E_f is the minor principal stress at failure divided by the minor principal strain at failure, where the maximum encountered hydrostatic stress and strain have been subtracted. The definition of E_f is given in eq. (3.8)

$$E_f = \frac{\sigma_{3f} - \sigma_{0,max}}{\epsilon_{3f} - \epsilon_{0,max}} \tag{3.8}$$

In [79.1] an equation for determining E_f is given. This original proposal has proven to yield too large values for E_f in the case of high strength concrete. The original proposal has therefore been modified and a new proposal is given in eq. (3.9).

$$E_f = \frac{E_c}{1 + 2\frac{E_0}{E_c}\left(\frac{\left(\sqrt{J_2}\right)_f}{f_c} - \frac{1}{\sqrt{3}}\right)} \tag{3.9}$$

In eq. (3.9) does the term $(\sqrt{J_2})_f$ denote the square-root of the invariant J_2 at failure, and is therefore connected to the actual loading and the determination of the non-linearity index, β. The term $[(\sqrt{J_2})_f/f_c - 1/\sqrt{3}]$ equals 0 in the uniaxial case, and eq. (3.9) therefore reduces to E_c in the case of uniaxial loading, as it should.

In Fig. 3.6 are eq. (3.9) shown compared to test results.

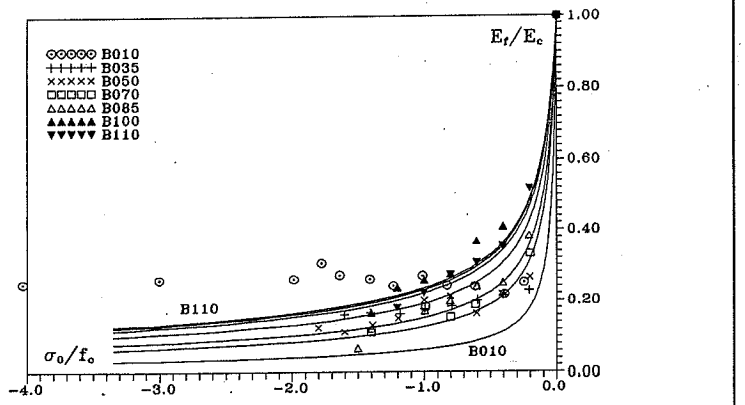

Fig. 3.6: Measured secant value at failure of Young's modulus compared to eq. (3.9).

It is seen that there is a good correlation between eq. (3.9) and the test results, except from concrete B010. It appears as if B010 is completely different from the rest of the concretes tested. This is most probably due to the very plastic stress-strain curve exhibited by B010 in conjunction with the limitations of the test equipment. As described in [92.2] the hydraulic jack will abort testing when the vertical deformation speed of the concrete specimen exceeds ~0.25 mm/s.

If the stress-strain curve has a very plastic appearance, as is the case with the very low strength concretes, the deformation speed will exceed the aborting value before the peak strain has been reached. The resulting E_f for these concretes will therefore be higher than the actual E_f, as is the case in Fig. 3.6. All in all does eq. (3.9) appear to yield sufficient accurate values for the secant value of Young's modulus at failure.

3.2.5 The apparent Poisson's ratio

In order to get the intermediate and major principal strain it is necessary to know the value of Poisson's ratio, ν. However, since the Poisson's ratio is a material constant it is only defined as long as no micro- or macro-cracking occur in the material. In concrete micro-cracks start forming at stresses less than the peak stress. Since the concrete strains are measured over a certain length of the concrete specimen it therefore follows that any crack appearing over the measuring length will influence the measurement of strain, and hence the ν-value. Therefore, in order to describe the deformations of concrete on a macroscopic scale the Poisson's ratio used will be an apparent Poisson's ratio called ν^a.

The observed effect of the influence of cracks on the Poisson's ratio is an increase in the apparent Poisson's ratio, and, for stresses near peak, a large scatter in the results. Furthermore, since the measured Poisson's ratio is an apparent value for stresses near peak, rather than a material constant, the measured Poisson's ratio can exceed the value of 0.5.

An example of this is displayed in Fig. 3.7 and 3.8. In these figures the apparent Poisson's ratio is displayed for all triaxial tests performed as a function of the major principal stress. In Fig. 3.7 the apparent Poisson's ratio at minimum volumetric strain is displayed. It can be seen that there is only a very small scatter in the results. This because only micro-cracks are present in the concrete specimens, and these cracks are very well dispersed in the concrete, hereby influencing both the vertical and the horizontal strain measurements.

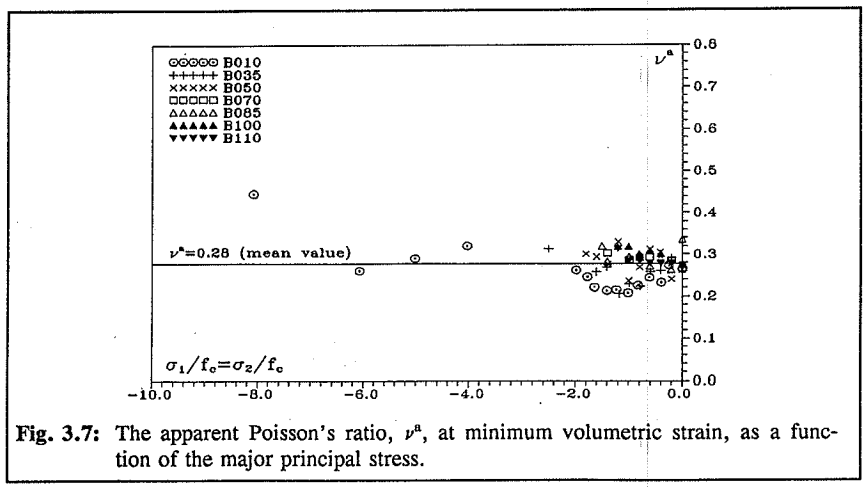

Fig. 3.7: The apparent Poisson's ratio, ν^a, at minimum volumetric strain, as a function of the major principal stress.

In Fig. 3.8 the apparent Poisson's ratio at failure is shown. Here the scatter of the results is much larger, and the apparent Poisson's ratio has in many cases exceeded 0.5.The reason for the large scatter and the, in some cases, very high Poisson's ratio, lies in the formation of macro-cracks. These cracks are not as well dispersed as the micro-cracks, and the opening of these cracks will therefore result in a larger scatter of the results, and in many cases a higher value of the apparent Poisson's ratio.

Several researchers have published results concerning the value of Poisson's ratio. Although a lot of research has been directed at determining the Poisson's ratio, no general agreement has been reached. Especially for high strength concrete there is a lot of disagreement, i.e. Neville [87.1]: ν=0.11; Chen [82.1]: ν=0.24. Also some disagreement exists for the low and

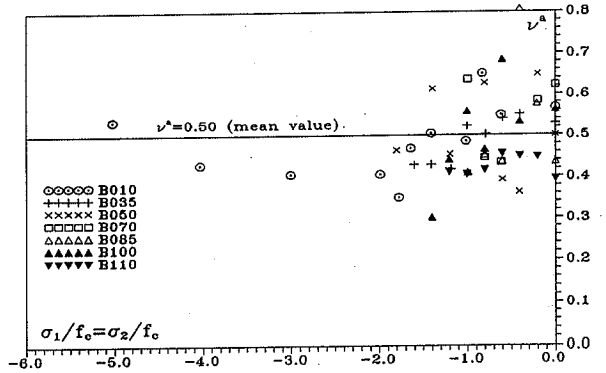

Fig. 3.8: The apparent Poisson's ratio, ν^a, at failure as a function of the major principal stress.

normal strength concretes, i.e. Ahmad & Shah [86.1]: ν=0.15; Neville [87.1]: ν=0.21.

The scatter at low stress ratios in the results of this investigation can be somewhat explained by the limitations of the measuring equipment. This because the major principal strains are not very large, and the numerical errors together with the limitations in the accuracy of the measuring equipment, will therefore influence the determination of Poisson's ratio. However, this does not explain all of the scatter in the test results. It is therefore more than possible that the Poisson's ratio depends on a number of other parameters, such as:

1/ the concrete strength,
2/ the aggregates,
3/ the loading speed,
4/ the principal stresses,
5/ the curing conditions etc.

The results from this investigation show that at least the parameters 1/ and 4/ have an influence on the apparent Poisson's ratio. In Fig. 3.9 and 3.10 are the apparent Poisson's ratio from tests with different major principal stresses compared. In Fig. 3.9 are the results of uniaxial and biaxial test shown, and in Fig. 3.10 are the results from triaxial tests with σ_1=0.6 f_c shown. It is seen that increasing the concrete strength will result in an increase in the initial value of the apparent Poisson's ratio, and increasing the major principal stress will result in a decrease in the initial value of the apparent Poisson's ratio.

The results of this program concerning the relation between concrete strength / major

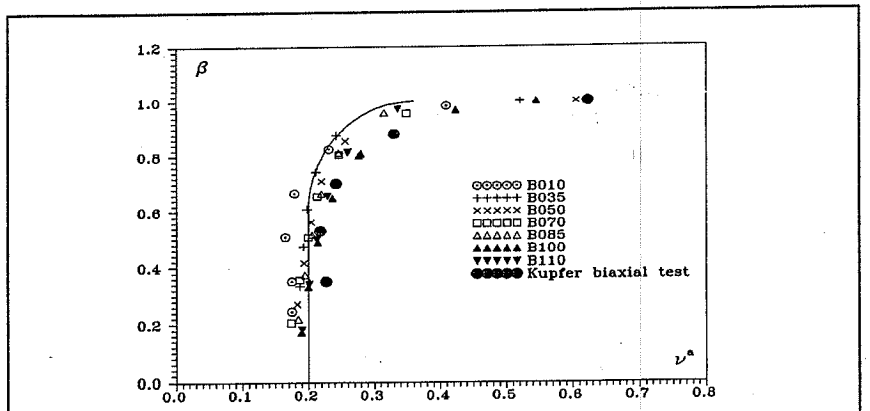

Fig. 3.9: The apparent Poisson's ratio for uniaxial and biaxial tests, compared to eq. (3.10) and (3.11)

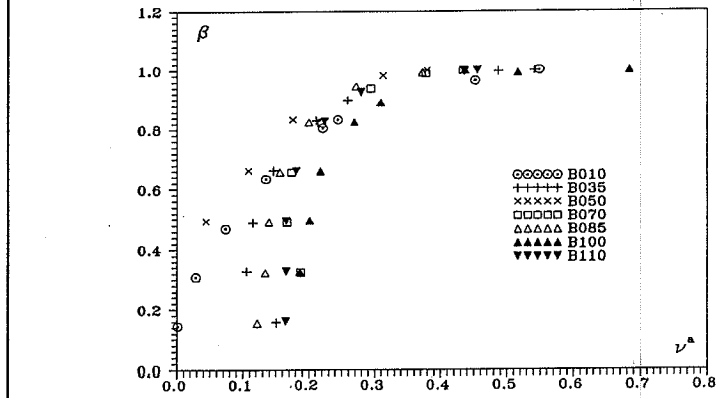

Fig. 3.10: The Poisson's ratio for the major principal stress σ_1=0.6 f_c.

principal stress and the apparent Poisson's ratio do not display any systematic tendencies. Therefore, no definite conclusion regarding these relations can be made. There is, however, a tendency for the initial value of the apparent Poisson's ratio to diminish for increasing major principal stress, and to increase for increasing concrete strength.

Generally the following statements concerning the apparent Poisson's ratio can be concluded:

1/ ν^a is constant until the stresses reach a certain limit of linearity, β_1.

2/ Beyond this limit of linearity ν^a is increased more and more rapidly.

3/ Measurements of ν^a are subject to some scatter, especially near the peak stresses.

Based on the above findings it has been found that eq. (3.10) represents the different test results well.

$$\nu^a = \begin{cases} \nu_i^a & \text{when } \beta \le \beta_l \\ \nu_f^a - (\nu_f^a - \nu_i^a)\sqrt{1 - \left(\dfrac{\beta - \beta_l}{1 - \beta_l}\right)^2} & \text{when } \beta > \beta_l \end{cases} \tag{3.10}$$

Eq. (3.10) is the equation suggested by Ottosen [79.1], where ν^a for $\beta > \beta_l$ is represented by one-quarter of an ellipse.

Also based on the above it has been found that there are differences between the apparent Poisson's ratio for triaxial loadings, as compared to the apparent Poisson's ratio for uniaxial and biaxial loadings. A reasonable accuracy is obtained if the following parameters are used:

<u>All loadings</u>

$$\beta_l = 0.6$$

<u>Uniaxial and biaxial loadings</u>

$$\nu_i^a = 0.20 \qquad \nu_f^a = 0.36 \tag{3.11}$$

<u>Triaxial loadings</u>

$$\nu_i^a = 0.15 \qquad \nu_f^a = 0.50$$

In Fig. 3.9 and 3.11 are eq. (3.10) and (3.11) shown together with test data. In Fig. 3.9 the apparent Poisson's ratio determined from uniaxial and biaxial test is shown, and in Fig. 3.11 the apparent Poisson's ratio determined from triaxial test is shown. In both figures the results from this investigation are compared to results from other researchers, and it can be seen that a reasonably good agreement exists.

However, there still remains quite a lot of research needed before any definite conclusion can be reached regarding the value of the apparent Poisson's ratio for any concrete subjected to any type of loading.

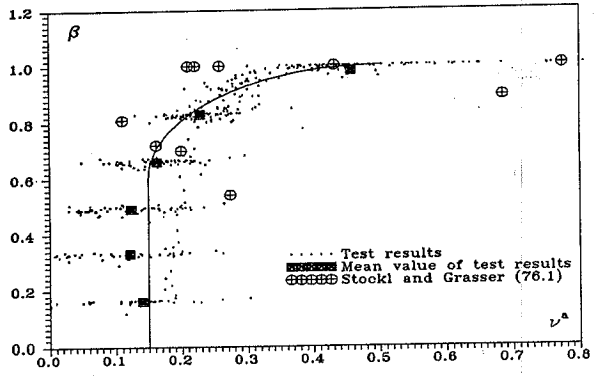

Fig. 3.11: The apparent Poisson's ratio for triaxial tests, compared to eq. (3.10) and (3.11).

3.3 Summary

In this chapter a constitutive model has been proposed. The model is based on the non-linear elastic theory, and is an improvement of the Ottosen model [79.1]. The model describes the short term deformations of concrete subjected to monotonously increasing compressive loads with or without prior hydrostatic loadings. The procedure for determining the deformations is as follows:

1/ The following parameters are needed to calibrate the model to the specific concrete.
   - a/ uniaxial concrete compressive strength, f_c
   - b/ initial value of Young's modulus, E_0
   - c/ the strain at peak stress, ϵ_c

   All 3 parameters can be determined from the standard uniaxial compression test.

2/ The strains for hydrostatic loading are determined using eq. (3.1).

3/ On basis of a failure criterion the minor principal stress at failure, σ_{3f}, is determined. This stress, in conjunction with the maximum pure hydrostatic stress previously encountered, $\sigma_{0,max}$, is used for calculating the non-linearity index β, eq. (3.2). As failure criterion the failure criterion of the author [92.2] will been used in this report. Any failure criterion can be used as stated earlier.

4/ The initial deviatoric Young's modulus, E_i, is determined using eq. (3.3), and the secant value of Young's modulus at failure, E_f, is determined using eq. (3.9). Based on E_i, E_f, and β, the secant value of the Young's modulus, E_s, at any given stress level can be determined using eq. (3.7).

5/ Using eq. (3.10), eq. (3.11), and the non-linearity index, β, the apparent value of Poisson's ratio, ν^a, can be determined.

6/ Using ν^a and E_s, the concrete strains can then be determined using eq. (3.12).

$$\epsilon_3 = \frac{\sigma_3 - \nu^a(\sigma_1 + \sigma_2)}{E_s}$$

$$\epsilon_2 = \frac{\sigma_2 - \nu^a(\sigma_3 + \sigma_1)}{E_s} \qquad (3.12)$$

$$\epsilon_1 = \frac{\sigma_1 - \nu^a(\sigma_2 + \sigma_3)}{E_s}$$

In the following chapter the constitutive model is validated by comparing its predicted strains to different experimental test results.

Chapter 4

Evaluation of the proposed model

In this chapter the constitutive model is compared to test data. In chapter 4.1 the model is compared to the test performed in this investigation. In chapter 4.2 and 4.3 is the model evaluated by comparing its stress-strain curves with test results from other investigations.

4.1 Comparison between the model and triaxial test results

The tests performed in this investigation have all been triaxial test loaded using the normal load path. The normal load path consists of loading along the hydrostatic axis ($\sigma_3=\sigma_2=\sigma_1$) until a predefined stress level is reached. Immediately after reaching the hydrostatic stress level the two major principal stresses are kept constant, and only the minor principal stress is increased until failure occurs.

In the following some of the triaxial test results will be compared to the model. During the investigation a number of uniaxial compression tests have also been performed. These stress-strain curves will not in this report be compared to the model. This because in the uniaxial case the model reduces to the expression suggested by CEB in [90.1], and this expression has been shown in [92.3], to compare very well with the uniaxial stress-strain curve of the same concretes as tested in this investigation.

In the Figures 4.1, 4.3, and 4.5 the model is compared to the stress-strain curves of concrete B035-3, B070-2 and B110-2. From each of these concretes a test performed with low-, medium-, and high hydrostatic stress level is compared to the model. Also in Fig. 4.2, 4.4, and 4.6 are the calculated volumetric strains compared to the model.

It is seen that the model generally is in very good agreement with the test results. The only main point of disagreement is that the initial deviatoric Young's modulus tends to be a little too high in the model for the low- and medium strength concretes subjected to high triaxial stresses. This is also what would be expected when examining Fig 3.5. However, all in all there seems to be a good correlation between the test results and the model, also when the

volumetric strains are examined.

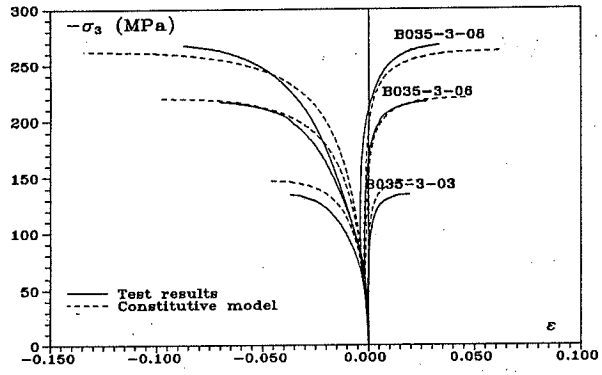

Fig. 4.1: Concrete B035-3, major and minor principal strains, compared to the model (normal load path).

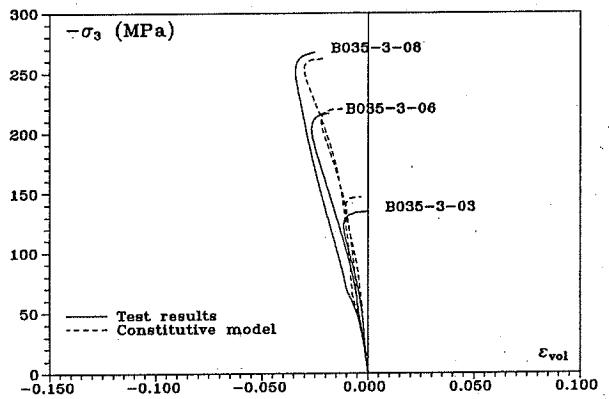

Fig. 4.2: Concrete B035-3, volumetric strains compared to the model (normal load path).

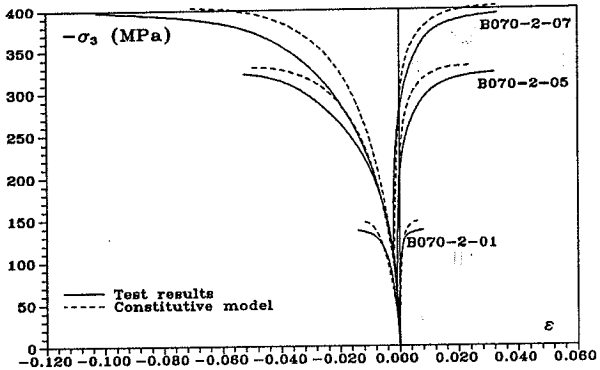

Fig. 4.3: Concrete B070-2, major and minor principal strains compared to the model (normal load path).

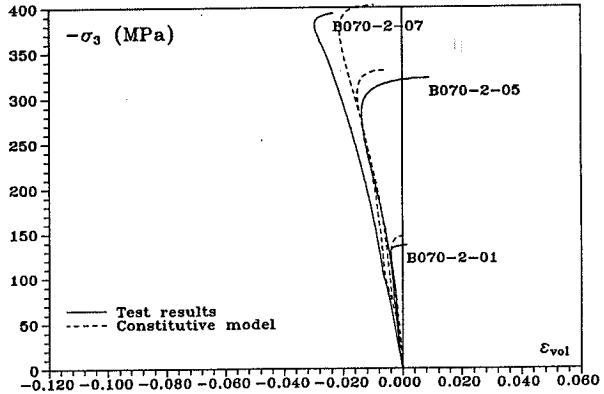

Fig. 4.4: Concrete B070-2, volumetric strains compared to the model (normal load path).

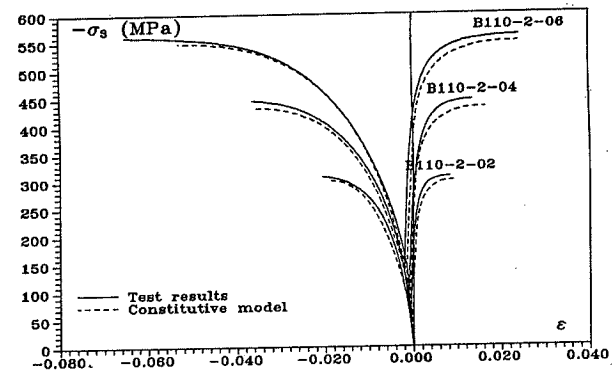

Fig. 4.5: Concrete B110-2, major and minor principal strains compared to the model (normal load path).

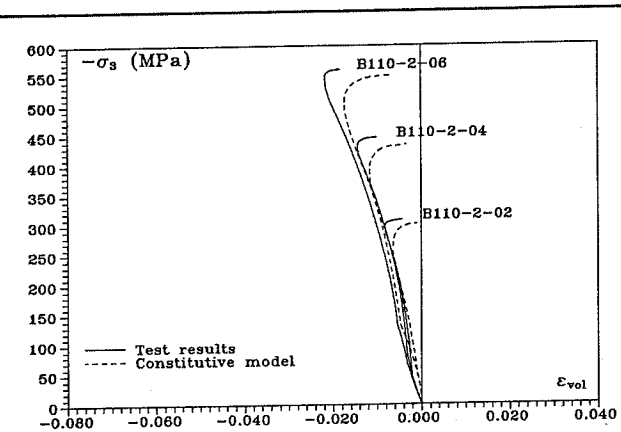

Fig. 4.6: Concrete B110-2, volumetric strains compared to the model (normal load path).

4.2 Comparison with other triaxial investigations

In order to evaluate the model properly, a thorough comparison with test data, other than the test data used in deriving the equations in the model, is needed.

This evaluation will be attempted in this chapter, where the results of most of the previously published test results are compared to the predictions of the model. Since the complete data sets of the stress-strain curves in the published test results are not available, the stress-strain curves have instead been digitalized. The points used in the digitalizing process are shown in each figure. The digitalizing process means that the stress-strain curves shown in this chapter are not exact but instead represent an approximation of the actual test results.

In the evaluation of the model, with respect to triaxial test results, the following investigations have been compared to the predictions of the model:

Normal load path
- Normal strength concrete
  - Hobbs [74.1], f_c= 31.8 MPa
  - Hobbs [74.1], f_c= 46.4 MPa
- High strength concrete
  - Ferrara et.al. [76.1], f_c= 56.9 MPa
  - Bellotti and Ronzoni [84.1], f_c=59.5 MPa
  - Newman and Newman [72.1], f_c= 73.3 MPa

Proportional load path
- Normal strength concrete
  - Stöckl and Grasser [76.2], f_c= 34.5 MPa
  - van Mier [84.3], f_c= 45.3 MPa

It has not been possible to compare the predictions of the model to high strength concretes loaded proportionally. This because no such investigations has to the author's knowledge been published.

4.2.1 Hobbs [74.1]

In Fig. 4.7 and 4.8 are the results of Hobbs compared to the predictions of the model. Hobbs used a cylindrical test specimen, tested using a normal load path, where the major and intermediate principal stresses were established using an oil pressure. The test rig was a typical cylindrical test rig and is the same in principle as the one used in this investigation,

see also [92.1]. In the figures the strains shown are not the major and minor principal strains but rather the deviatoric strains, meaning that the maximum hydrostatic strain is subtracted from the principal strains.

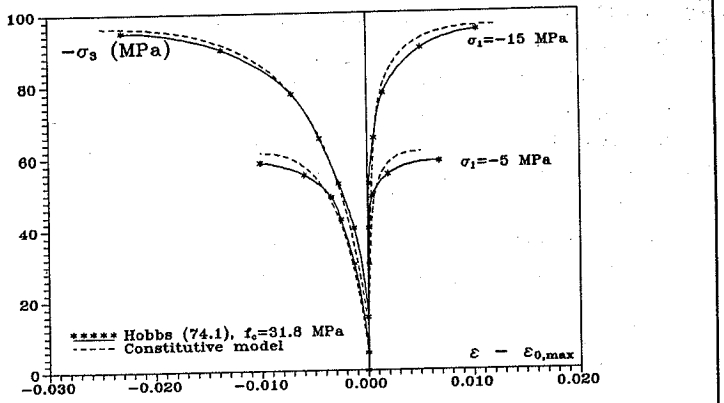

Fig. 4.7: Hobbs [74.1], normal load path.

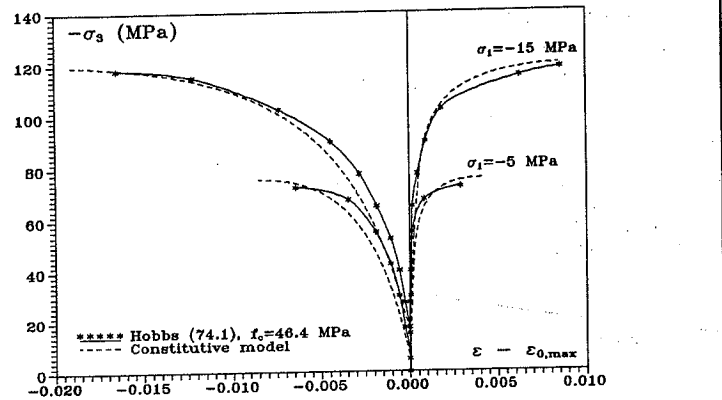

Fig. 4.8: Hobbs [74.1], normal load path.

Hobbs has not provided all of the parameters needed for calibrating the model. The necessary

parameters have therefore been estimated to be as follows:

f_c= 31.8 MPa: E_i= 27000 MPa, ϵ_c= 0.00216
f_c= 46.4 MPa: E_i= 37000 MPa, ϵ_c= 0.00250

It is seen in the figures that the prediction of the model corresponds very well with the test results. The only discrepancy between the model and the test results is that the initial deviatoric Young's modulus of the model in some cases seems to be a little lower than the test results indicate.

4.2.2 Ferrara et.al. [76.1]

The test results of Ferrara et.al. are shown in Fig. 4.9. The load path is assumed to be a normal load path, and the test specimen and test rig is assumed to be of the same type as used by Hobbs [74.1].

The parameters used for calibrating the model have been estimated to be:

f_c= 56.9 MPa, E_i= 44000 MPa, ϵ_c= 0.00216

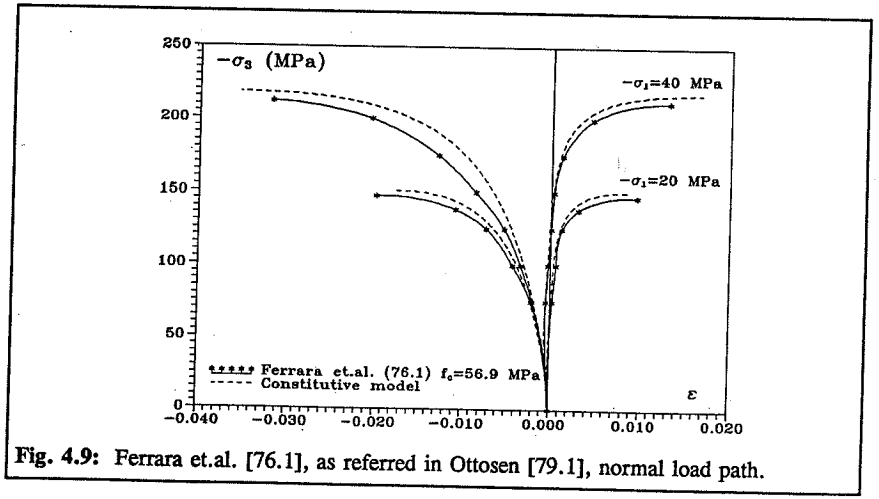

Fig. 4.9: Ferrara et.al. [76.1], as referred in Ottosen [79.1], normal load path.

It is seen that model in all respects yields a close fit to the test results.

4.2.3 Bellotti and Ronzoni [84.1]

In Fig. 4.10 are shown the results of Bellotti and Ronzoni. The test specimen, load path, and test rig used are of the same type as used by Hobbs [74.1].

As parameters for the model, the following have been used:

f_c= 59.5 MPa, E_i= 38000 MPa, ϵ_c= 0.00300

Again it is seen that the model is in very close agreement with the test results. Only the strain at peak stress seems to be a little high. However, as described previously this value is very hard to determine correctly. This because it requires a very stiff test environment in order to catch the last, almost horizontal, part of the stress-strain curve. In uniaxial tests this does not present a major problem as far as high strength concrete is concerned, however, the very ductile behavior of any type of concrete under high triaxial stresses makes the last part of the stress-strain curve very difficult to determine experimentally.

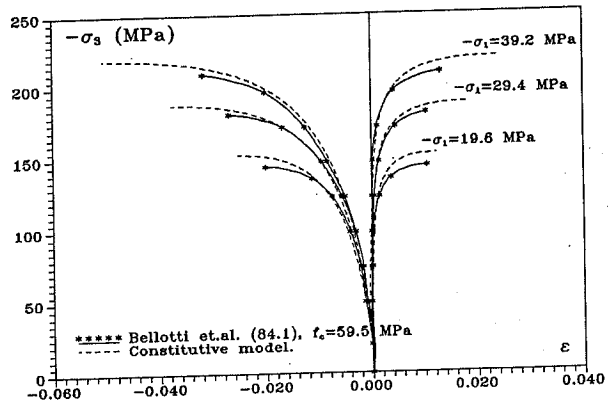

Fig. 4.10: Bellotti and Ronzoni [84.1], normal load path.

4.2.4 Newman and Newman [72.1]

The results of J.B. Newman and K. Newman are shown in Fig. 4.11. The test specimen, load path, and test rig used are of the same type as used by Hobbs [74.1].

It has not been possible to determine the parameters for calibrating the model other than the compressive strength of the concrete. Therefore, as an estimation, the following parameters have been used. These parameters are based on the equations determined by the author in [92.3].

f_c= 73.3 MPa: E_i= 37400 MPa, ϵ_c= 0.00270

In the figure the principal strains versus the actual principal stress is shown. The actual stress is not the same stress as is used in the remaining figures in this report. Normally the stresses are calculated as the force divided by the area of the concrete in the undeformed specimen. In the case of Newman & Newman, the actual stress has been calculated as the force divided by the area of the concrete in the deformed specimen where the deformations are given by the major principal strain.

In Fig. 4.11 it is seen that the model yields a good estimate of the concrete strains, even for the specimen loaded with very high hydrostatic stress.

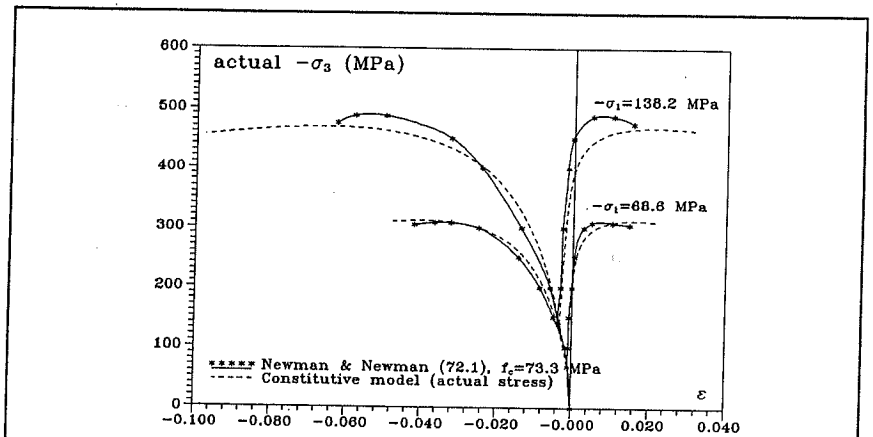

Fig. 4.11: Newman and Newman [72.1], normal load path.

4.2.5 Stöckl and Grasser [76.2]

In Fig. 4.12 and 4.13 are the results of Stöckl and Grasser shown. The tests were carried out on concrete cubes, using a proportional load path where the intermediate and the major

principal stresses were kept equal. The test rig used was a one-part triaxial testing machine were the jacks are in a fixed position at all times. It has been shown, i.e. by van Mier [84.3], that using a one-part machine will influence both the strength and also the deformations of the concrete specimen, as opposed to using a multi-part machine. The influence on the deformations should be highest on the major principal strains because of the tendency of the specimen to be pushed into a corner. The problem is described in more detail in [90.2] and [85.1].

Another problem concerning testing of concrete cubes is the known difference between the strength test results of cubes as compared to cylinders. This difference has not yet been fully understood or explained. One of the differences is the tendency for cylinders to yield a slightly higher triaxial strength as compared to cube tests where brush-type load plates have been used. A more thorough discussion of this subject can be found in [92.2] or [91.2].

The reason for including cube tests in general, and the results of Stöckl and Grasser in particular, is that very few stress-strain curves of proportionally loaded cylinders have been published. Therefore, in order to verify ability of the model to predict the stresses for loadings other than the normal load path, the tests of Stöckl & Grasser and the tests of van Mier have been included.

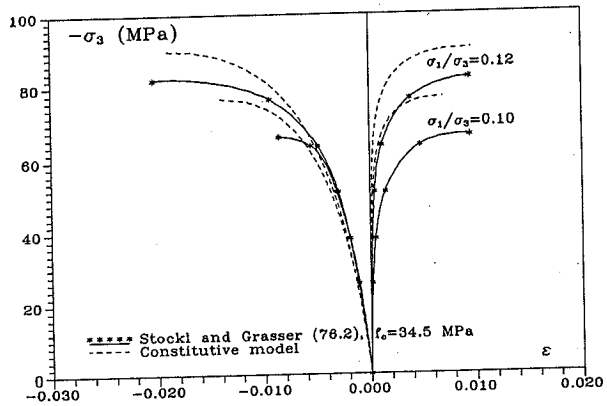

Fig. 4.12: Stöckl and Grasser [76.2], proportional load path.

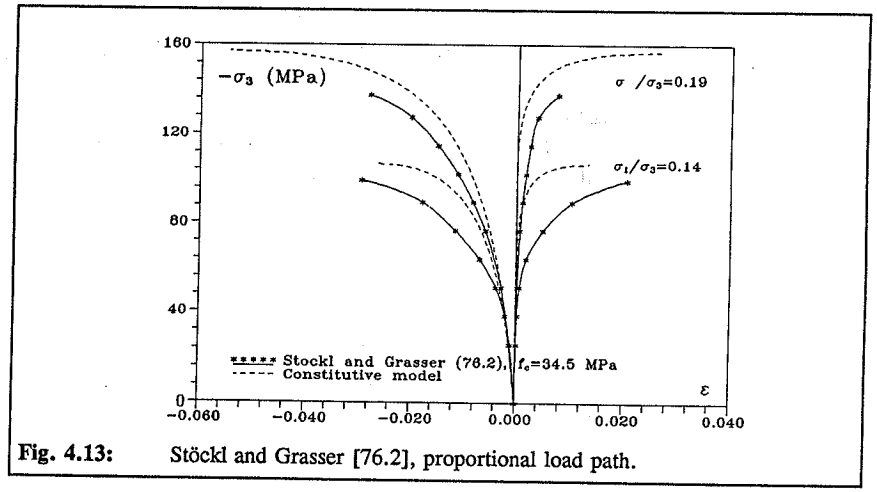

Fig. 4.13: Stöckl and Grasser [76.2], proportional load path.

As parameters for calibrating the model, the following have been used:

f_c= 34.52 MPa, E_i= 24000 MPa, ϵ_c= 0.00240

Examining the figures it is seen that the deviation between the model and the test results is not excessive for the minor principal strains, except for the fact that the model generally overestimates the peak stress. In the case of the major principal strains, the test results show a more soft behavior than the predictions of the model. These differences can be explained by the influence of the test rig on the measured strains as previously described.

4.2.6 van Mier [84.3]

In Fig. 4.14 are the results of van Mier [84.3] shown. The concrete specimen tested was a cube, loaded using a proportional load path where the intermediate and major principal stresses were kept equal. van Mier used a multi-part triaxial test machine, as opposed to the one-part test machine used by Stöckl and Grasser.

As parameters for calibrating the model, the following have been used:

f_c= 45.30 MPa, E_i= 40300 MPa, ϵ_c= 0.00200

It is seen in Fig. 4.14 that the predictions of the model correspond well to the test results apart from the value of the peak stress. It can also be seen that the results of van Mier show

a more stiff behavior for the major principal strains when compared to the results of Stöckl and Grasser, which lends validity to the above mentioned differences between a one-part and a multi-part test machine.

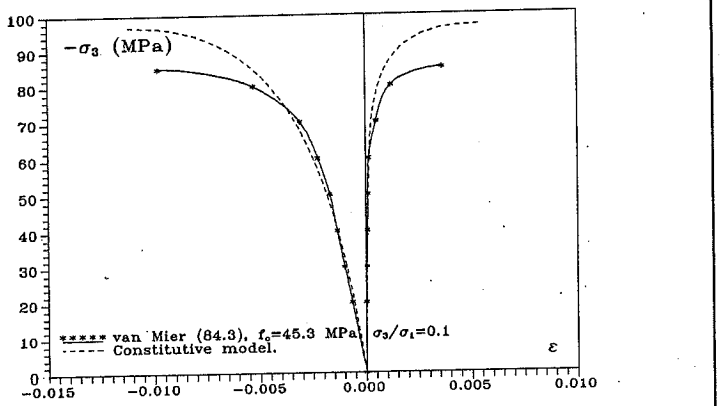

Fig. 4.14: van Mier [84.3], proportional load path.

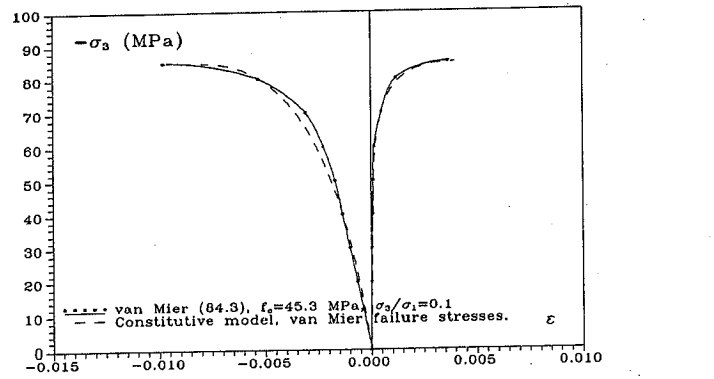

Fig. 4.15: van Mier [84.3], proportional test data, the failure stresses of van Mier used as failure criterion.

In Fig. 4.15 the model is changed in that the peak value of the stresses of that particular test

is used as the failure stresses rather than the predictions of the failure criterion normally employed. This is done in order to check whether the differences between the model and the test results can be ascribed to the failure stresses or are due to errors in the constitutive model. It is obvious, when examining Fig 4.15, that the differences in this case must be accredited to the difference in the value of the failure stresses rather than to errors in the model.

van Mier has also performed tests using a proportional load path, where the intermediate and the major principal stresses were not equal. These tests are shown in Fig. 4.16 - 4.18, where also the principal stress ratios are given.

In these tests it is seen that the model predicts the stress-strain curves in an acceptable way. The only discordance lies in the intermediate principal strain near peak stress. The model tends to let the intermediate principal strain approach the major principal strain for an increasing difference between the corresponding principal stresses. This discordance, however, is seen only near peak stress. For stresses below peak stress there is a good accordance between the model and the test results.

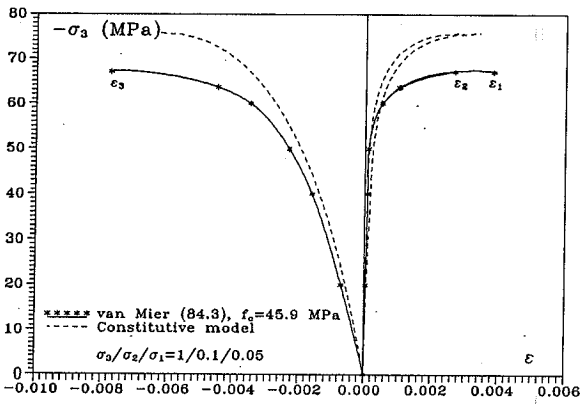

Fig. 4.16: van Mier [84.3], proportional load path, $\sigma_3/\sigma_2/\sigma_1$ = 1/0.1/0.05.

This is an error of the model and is due to the determination of the apparent Poisson's ratio. If the model is to be valid for large differences between the intermediate principal stress and the major principal stress, the relation between the apparent Poisson's ratio and the principal stresses has to be determined. This relation lies outside the scope of this investigation, and

calls for a more thorough general investigation into the parameters that affects the apparent Poisson's ratio, as described in chapter 3.

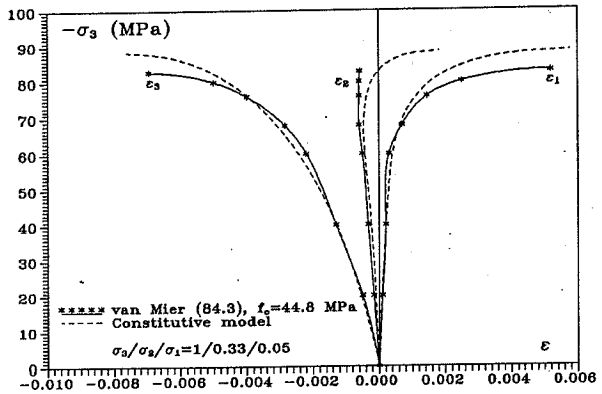

Fig. 4.17: van Mier [84.3], proportional load path, $\sigma_3/\sigma_2/\sigma_1$ = 1/0.33/0.05.

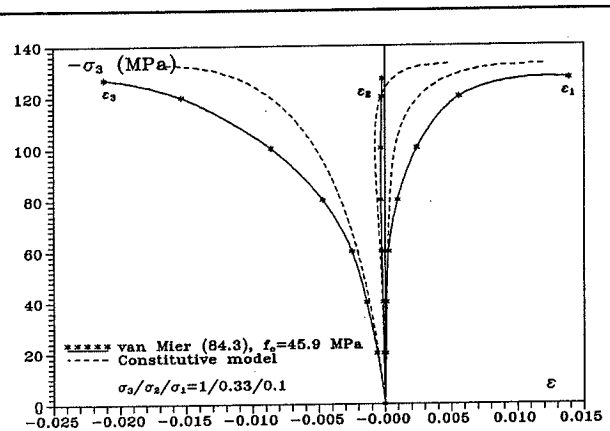

Fig. 4.18: van Mier [84.3], proportional load path, $\sigma_3/\sigma_2/\sigma_1$ = 1/0.33/0.1.

4.3 Comparison with biaxial test results

In chapter 4.1 and 4.2 is the model compared to triaxial test results, and in [92.3] with uniaxial test results. Left now is only to compare the model with biaxial test results. This will be attempted in this chapter. The model is compared to the results of Kupfer [73.1]. Kupfer tested both normal and high strength concretes, and the investigation is generally thought to be one of the most comprehensive and correct biaxial test programs ever performed.

Kupfer used a concrete plate 200·200·50 mm as test specimen loaded using a proportional load path. The test rig was designed as a multi-part testing machine in order to minimize the influence of the test rig on the test results.

4.3.1 Kupfer, [73.1], normal strength concrete

In Fig. 4.19 and 4.20 are the test results of 4 different specimens shown. The load paths used ranges from $\sigma_3/\sigma_2/\sigma_1$ = 1/0/0 to 1/1/0. As parameters for calibration of the model, the following have been used, as specified in [73.1].

$$f_c = 31.80 \text{ MPa}, \quad E_i = 32400 \text{ MPa}, \quad \epsilon_c = 0.00216$$

It is seen, apart from a slight overestimation of the biaxial strength in some cases, that the model is in very good agreement with the test results.

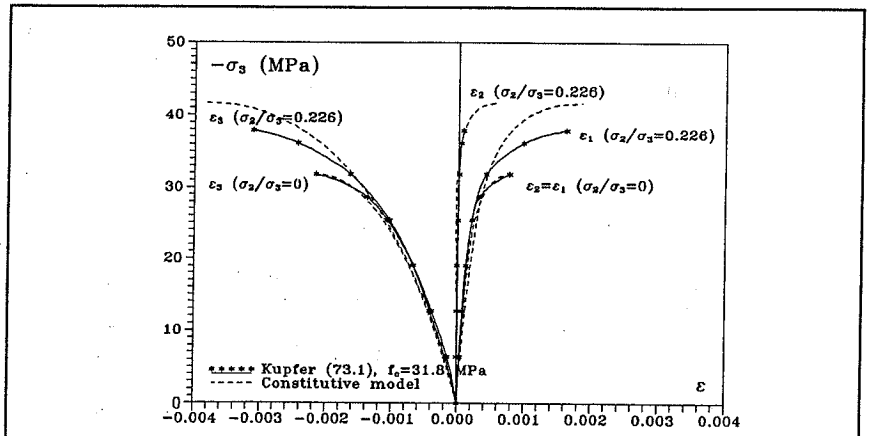

Fig. 4.19: Kupfer [73.1], normal strength concrete in biaxial compression.

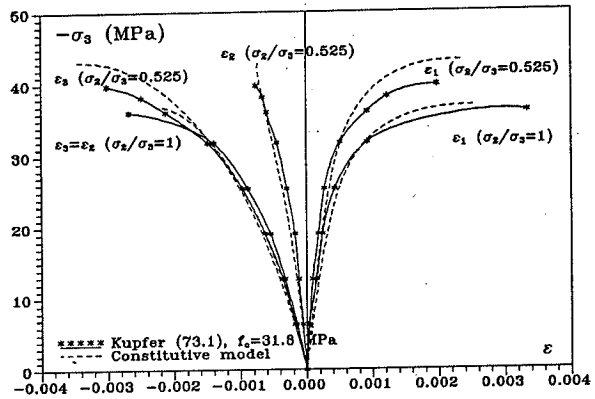

Fig. 4.20: Kupfer [73.1], normal strength concrete in biaxial compression

Shown in Fig. 4.21 are the volumetric strains. In the figure an almost complete accordance between the test results and the model is observed.

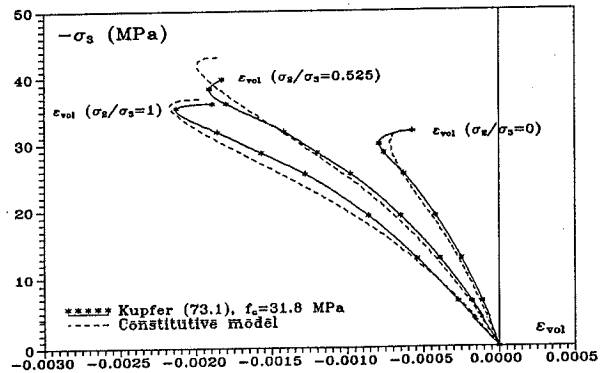

Fig. 4.21: Kupfer [73.1], volumetric strains of normal strength concrete in biaxial compression.

4.3.2 Kupfer, [73.1], high strength concrete

In Fig. 4.22 and 4.23 the test results of 4 different specimens are shown. The load paths used ranges from $\sigma_3/\sigma_2/\sigma_1$ = 1/0/0 to 1/1/0. As parameters for calibration of the model, the following have been used, as specified in [73.1].

$$f_c = 60.70 \text{ MPa}, \quad E_i = 39200 \text{ MPa}, \quad \epsilon_c = 0.00214$$

It is seen, apart from the intermediate principal strains very close to failure of some of the specimens, that the model is in very good agreement with the test results. The disagreement is due to the equation for the apparent Poisson's ratio, which has not been adequately determined as a function of the load path and the stress ratios. The problem is therefore an error in the model, and is similar to the problem described in chapter 4.2.6.

The disagreement mostly results in an intermediate principal strain curve that close to failure starts curving towards an extension rather than a compression.

However, all in all there seems to be a good accordance between the model and the test results.

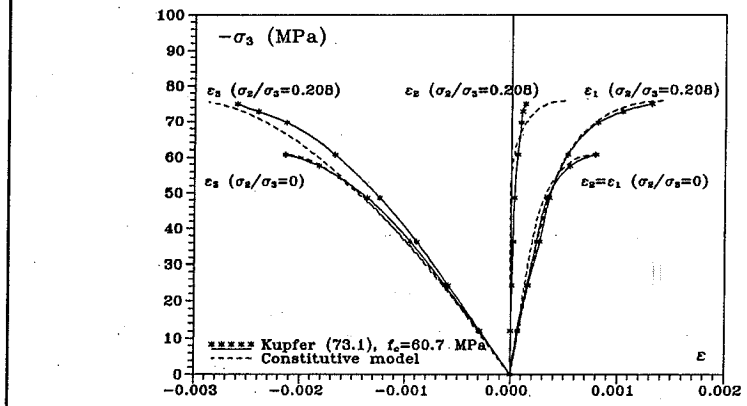

Fig. 4.22: Kupfer [73.1], high strength concrete in biaxial compression.

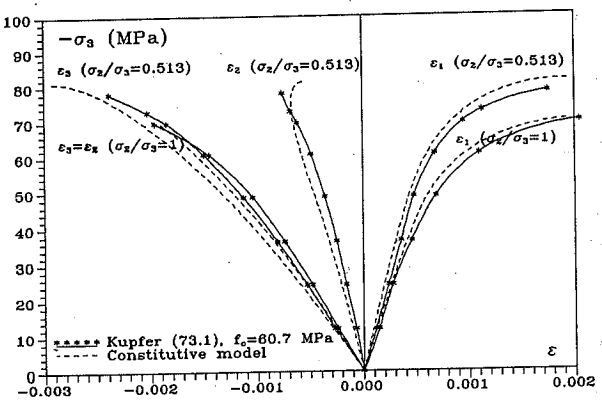

Fig. 4.23: Kupfer [73.1], high strength concrete in biaxial compression.

4.4 Summary of verification

In the preceding chapter the proposed constitutive model has been validated by comparing its predicted stress-strain curves to test results from many different investigations. The different investigations have employed a variety of concretes, test rigs, load paths, and specimen types. Even without taking these many differences into account it is seen that the proposed constitutive equation yields very good predictions of the strain in concrete subjected to generalized loadings.

The only problem encountered is when the difference between the major and the intermediate principal stresses becomes large. In these cases will the predictions of the intermediate principal strain suffer somewhat for stresses near the failure stresses. This behavior is due to the equation governing the value of the apparent Poisson's ratio. As described in chapter 3 there are many parameters that govern the apparent Poisson's ratio, and the influence of all of these parameters has not yet been investigated.

In chapter 3 a proposed equation for the apparent Poisson's ratio is stated. Because this investigation has not been directed towards a more accurate determination of the apparent Poisson's ratio, only a very simple modelling of this aspect of concrete behavior has been attempted. If the proposed constitutive model is to be improved, much of the necessary

research has to be directed towards a better understanding of the parameters that influence the apparent Poisson's ratio.

All in all, however, the proposed constitutive model relates very well to the deformational behavior of concrete with the following limitations:

1/ The constitutive model covers monotonously increasing compressive loads, with or without prior hydrostatic loadings.

2/ The constitutive model is valid for normal concretes, is does not consider lightweight nor fiber reinforced concretes.

3/ The constitutive model is valid for concrete with an uniaxial compressive strength up to 100 MPa.

4/ The constitutive model is valid for the major and intermediate principal stresses in the range 0 to 120 MPa.

5/ The constitutive model is valid only for short-time loadings. The model does not include effects of time on the deformational response of concrete.

6/ At the present the model does not consider tensile loadings, nor the descending branch of the stress-strain curve. This, however, is fairly simple to implement in the model, as shown by Ottosen in [79.1].

Chapter 5

Concrete versus mortar

Parallel to the investigation of the influence of the concrete strength on the deformational response, an number of pilot tests were performed to investigate the influence of the aggregates also on the deformational response of concrete. Two mortar mixes and one paste mix were cast and tested in the same way as the concrete specimens.

In appendix 1 the stress-stain curves of these tests are shown, and in appendix 2 the main results are stated. It has to be noted that the paste test results deviate from the mortar test results in that the paste specimens were severely damaged due to shrinkage cracks. The strain measurements of the paste cylinders are therefore in some way influenced by these shrinkage cracks. No exact value can be attached to the influence of the shrinkage cracks, therefore the strain measurements on the paste cylinders are only considered as a guide to the real strains in the paste. As a consequence, the stress-strain curves of the paste specimens are shown in appendix 1, but the corresponding experimental results are not stated in appendix 2.

The shrinkage cracks also influenced the uniaxial compressive strength of the paste specimens. This is further described in [92.2].

The main results of the investigation into the influence of the aggregate content are as follows:

- The strain at peak stress under triaxial loadings is increased when the aggregate content is lowered. This is parallel to the results of the uniaxial compression test as found in [92.3].

- When approaching peak stress the specimens did show decreasing dilatation for decreasing aggregate content corresponding to a decrease in the apparent Poisson's ratio at failure, ν_f^a.

- When the aggregate content was lowered the specimens did show a distinct change in the stress-strain curve. This change is especially visible in the tests of mortar M070A or the paste P070, where the stress-strain curves almost can be

said to consist of two or three phases in which the minor principal stress-strain curve is almost linear.

A theory that can somewhat explain the above described behavior is as follows. The stress concentrations around the aggregate particles will result in the material strength being exceeded in small areas in the concrete, resulting in micro-cracks occurring. If the material is made more homogeneous these stress concentrations will diminish and the range of stress in which cracking starts will be shortened and appear at a later stage. This will influence the stress-strain curve in that it will become less curved in most places, and more curved in a few places.

The more homogeneous the material is the more the deformational response will then consist of three distinct phases:

1/ an 'elastic' phase were no cracking occurs

2/ a 'cracking' phase where cracks occur leading to irreversible deformations

3/ a 'yielding' phase where larger and more coherent crack systems appear leading to failure.

These phases are connected to the 'Onset of Stable Fracture Propagation', OSFP-level, and 'Onset of Unstable Fracture Propagation', OUFP-level, as described i.e. by Chen [82.1]. In normal concrete especially the OSFP-level is hard to determine. This because the stress concentrations around the aggregate particles will result in cracking occurring at different stress levels at different locations inside the specimen. The resulting stress-strain curve will then exhibit a smooth curvature.

In the case of a more homogeneous material, such as hardened cement paste, there are no large particles to create these stress concentrations. The OSFP-level will then tend to be reached for a more well defined stress level than is the case for normal concrete. The resulting stress-strain curve will therefore, as a consequence, exhibit a more distinct linear behavior between the OSFP-level and the OUFP-level.

If the analogy is carried into a very homogeneous material such as steel the OSFP-level can be viewed as the level where yielding takes place. The influence of the aggregate content on the deformational response of concrete then follows the same trend as the influence of the aggregate content on the failure strength of concrete as described in [92.2], that is the more homogenous the material is, the more alike to steel it behaves.

It must be emphasized, however, that the test results of this investigation do not present conclusive evidence concerning the above mentioned theory. At the most the experimental evidence hints at the theory being somewhat correct.

Chapter 6

Conclusion

In this report an improvement of the Ottosen constitutive model for short time loadings has been proposed. The model is valid for monotonously increasing compressive loads, with or without prior hydrostatic loadings. The constitutive model is based on the nonlinear elastic theory where the secant value of the apparent Poisson's ratio, and the secant value of Young's modulus is changed appropriately.

The model is made independent of the failure stresses by means of the non-linearity index, β, and can therefore be used in conjunction with any failure criterion. The constitutive model supplies realistic and smooth stress-strain curves for any type of compressive loadings, including uniaxial, biaxial, and triaxial loadings. Only for stress states where the intermediate and the major principal stresses deviate significantly from each other does the model fail to predict realistic intermediate principal strains, and then only for stresses near the peak value.

The model is calibrated to the particular concrete by means of the 3 parameters:

- uniaxial concrete strength, f_c
- initial Young's modulus, E_0
- strain at peak stress in uniaxial compression, ϵ_c

The calibration process is easily performed as the 3 parameters can be determined by the standard uniaxial compression test.

The constitutive model is valid for normal concretes having an uniaxial strength up to 100 MPa, and for the intermediate and major principal stress in the range 0 to 120 MPa.

It has been shown that the predictions of the model is in very good agreement with test results from other researchers. The comparisons have been performed on a wide range of different test equipments, a wide range of stress states, and on widely different concretes. In all cases were the predictions of the model well within acceptable limits of the test results.

References

[65.1] ***Behavior of Plain Concrete Under Various High Triaxial Compression Loading Conditions.***
J. Chinn and R.M. Zimmerman, Air Force Weapons Lab. Tech. Rep. WL TR 64-163, Kirtland Air Force Base, New Mexico, 1965.

[72.1] ***The Cracking and Failure of Concrete Under Combined Stresses and its Implications for Structural Design.***
J.B. Newman and K. Newman, The Deformations and Rupture of Solids Subjected to Multiaxial Stresses, RILEM international symposium, Cannes, October, 1972.

[73.1] ***Das Verhalten des Betons unter mehrachsiger Kurzzeitbelastung unter besonderer Berücksichtigung der zweiachsigen Beanspruchung.***
H. Kupfer, Deutscher Ausschuss für Stahlbeton, heft 229, 1973.

[74.1] ***Strength and Deformation Properties of Plain Concrete Subject to Combined Stress. Part 3: Results Obtained on a Range of Flint Gravel Aggregate Concretes.***
D.W. Hobbs, Cement and Concrete Association, report 42.497, July 1974.

[76.1] ***Dispositivi di prova per l'analisi sperimentale del comportamento do conglomerati cementizi sottoposti a stati triassaili di sollecitazione.***
G. Ferrara et.al., presented at the October 1976, 4th Associazione Italiana Annalisi Sollecitazione Congress, held at Rome, Italy.

[76.2] ***Versuche zum Verhalten von Beton unter Mehrachsiger Beanspruchen.***
S. Stöckl and E. Grasser, Technische Universität München, internal report, May 1976.

[78.1] ***Generalized Stress-Strain Relations for Concrete.***
M.D. Kotsovos and J.B. Newman, Journal of the Engineering Mechanics Division, August 1978, EM4, pp. 845 - 856.

[79.1] *Constitutive Model for Short-Time Loading of Concrete.*
N.S. Ottosen, Journal of the Engineering Mechanics Division, February 1979, EM1, pp. 127 - 141.

[79.2] *Plastic-Fracturing Theory of Concrete.*
Z.P. Bazânt and S-S. Kim, Journal of the Engineering Mechanics Division, ASCE, vol. 105, no. EM3, June 1979, pp. 407-428.

[82.1] *Plasticity in Reinforced Concrete.*
W.F. Chen, McGraw-Hill Book Company, New York, 1982.

[84.1] *Results of Tests Carried out on Cylindrical Concrete Specimens Subjected to Complex Stress States: A Critical Analysis.*
R. Bellotti and E. Ronzoni, International Conference on Concrete under Multiaxial Conditions, RILEM, Press de l'Universite Paul Sabatier, Toulouse, May 1984, pp 9 - 19.

[84.2] *DS 423.23. Betonprøvning, Hærdnet beton, Trykstyrke.*
Dansk Standard, DS 423.23, 1984.

[84.3] *Strain-Softening of Concrete under Multiaxial Loading Conditions.*
J.G.M. van Mier, Doctoral thesis, Eindhoven, Holland, 1984.

[85.1] *Grundsätzliche Untersuchungen zum Geräteeinfluss bei der mehraxialen Druckprüfung von Beton.*
H. Winkler, Deutscher Ausschuss für Stahlbeton, heft 366, 1985.

[86.1] *Orthotropic Model of Concrete for Triaxial Stresses.*
S.H. Ahmad, S.P. Shah and A.R. Khaloo, Journal of Structural Engineering ASCE, vol 112, no.1, January 1986, pp. 165 - 181.

[87.1] *Properties of Concrete, 3'rd edition.*
A.M. Neville, Longman Scientific & Technical, England, 1987.

[90.1] *CEB model code 1990.*
Comite Euro-International du Beton, Bulletin d'Information no 203, 1991.

[90.2] *Preliminary State-of-the-art Report on Multiaxial Strength of Concrete.*
Kaare K. B. Dahl, Department of Structural Engineering, Technical University of Denmark, Report R 262, 1990. Also published in 'Højkvalitetsbetoner i 90'erne', Report 5.1.

[91.1] *Comments on Major Constitutive Models for Concrete.*
S-S. Kim, Technical University of Denmark, published in 'Højkvalitetsbetoner i 90'erne', Report 5.4, 1991.

[91.2] *Multiaxial Testing of Concrete.*
RILEM Technical Committee, Final Report, Materials and Structures, vol. 24, no. 139, 1991, pp. 38 - 69.

[92.1] *The Calibration and Use of a Triaxial Cell.*
Kaare K. B. Dahl, Department of Structural Engineering, Technical University of Denmark, Report R 285, 1992. Also published in 'Højkvalitetsbetoner i 90'erne', Report 5.5.

[92.2] *A Failure Criterion for Normal and High Strength Concrete.*
Kaare K. B. Dahl, Deptartment of Structural Engineering, Technical University of Denmark, Report R 286, 1992. Also published in 'Højkvalitetsbetoner i 90'erne', Report 5.6.

[92.3] *Uniaxial Stress-Strain Curves for Normal and High Strength Concrete.*
Kaare K. B. Dahl, Department of Structural Engineering, Technical University of Denmark, Report R 282, 1992. Also published in 'Højkvalitetsbetoner i 90'erne', Report 7.6.

Appendix 1

Strain diagrams

In this appendix are given the strain measurements on all the tested concrete cylinders. The strains are graphically shown in a (σ,ϵ)-system where the stress, σ, is the minor principal stress σ_3. In this report tension stresses are assumed positive. For the strains extension is assumed positive.

In the graphs in this appendix all the test cylinders from a single batch have been shown together, however, in the case of B010 this was not possible, and in this case the strains have been shown in two different graphs. For each batch the graphs shown are:

1/ The longitudinal strain, ϵ_3, versus the minor principal stress, σ_3.
2/ The vertical strain, ϵ_1, versus the minor principal stress, σ_3.
3/ The volumetric strain, ϵ_{vol}, versus the minor principal stress, σ_3.

At the end of each curve a number is shown. This number is the normalized level of hydrostatic pressure, σ_1/f_c, at which the test was conducted. In some cases this number is followed by an asterisks, denoting that the measurement was stopped prior to failure of the concrete. This means that both of the strain gauges on that particular concrete cylinder, and in that particular direction, failed at some point during the test.

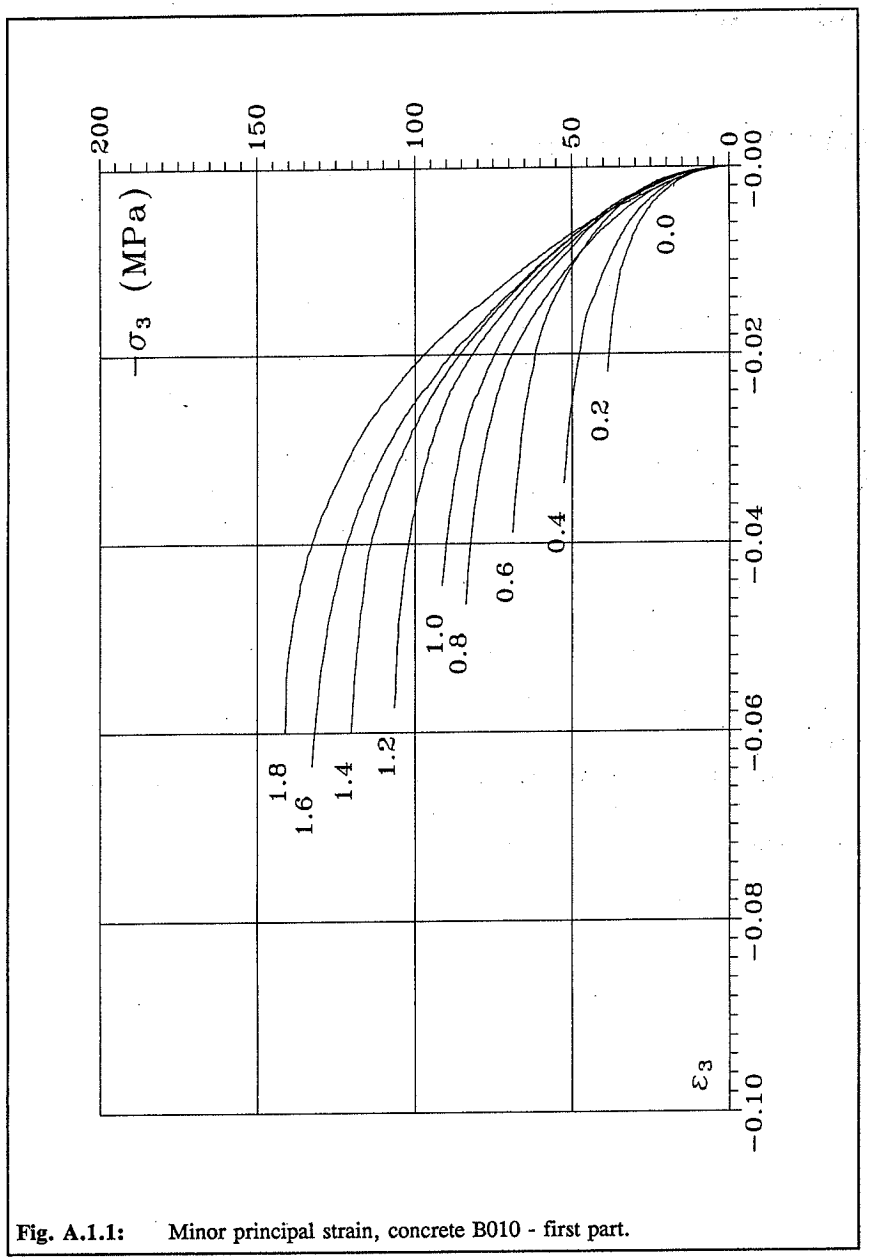

Fig. A.1.1: Minor principal strain, concrete B010 - first part.

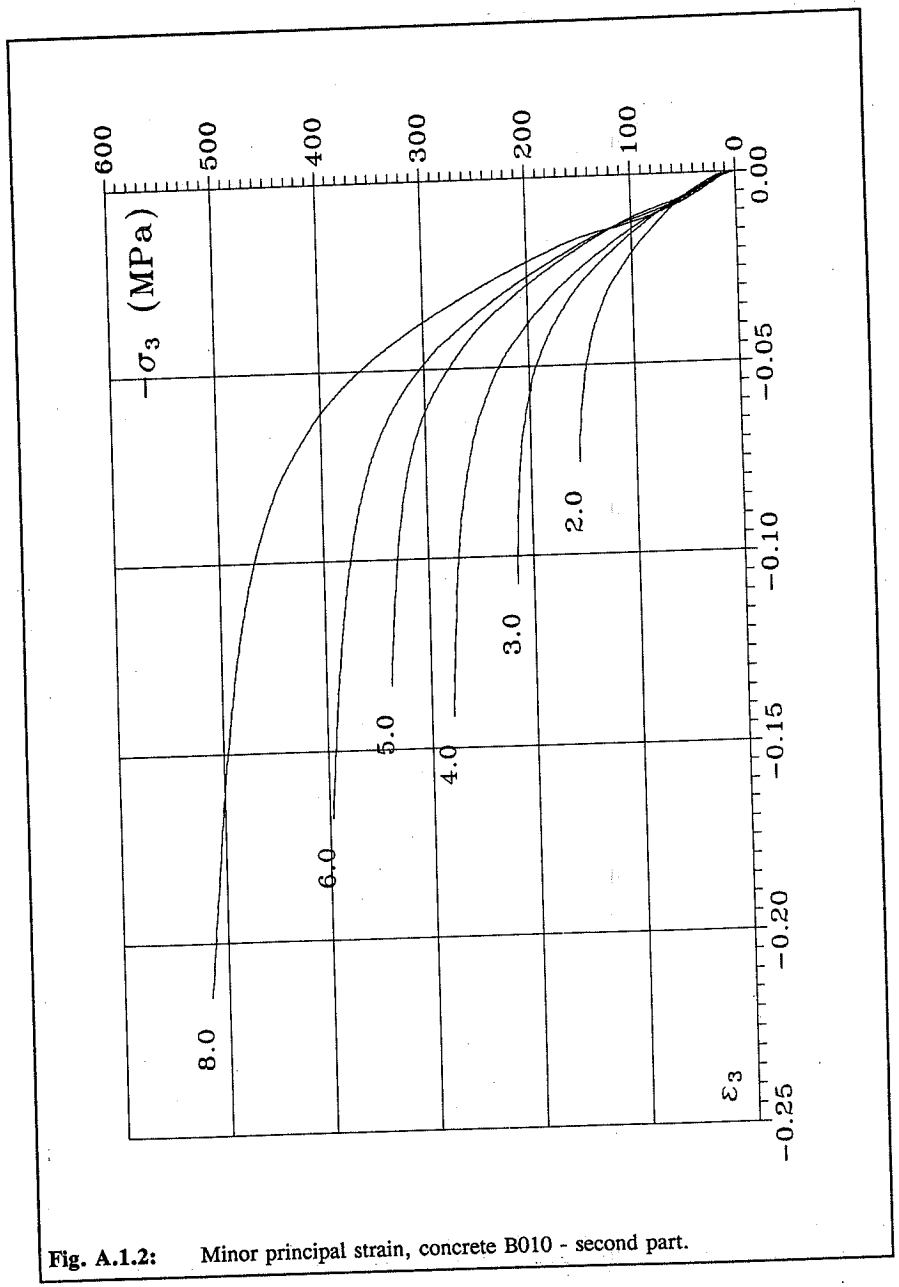

Fig. A.1.2: Minor principal strain, concrete B010 - second part.

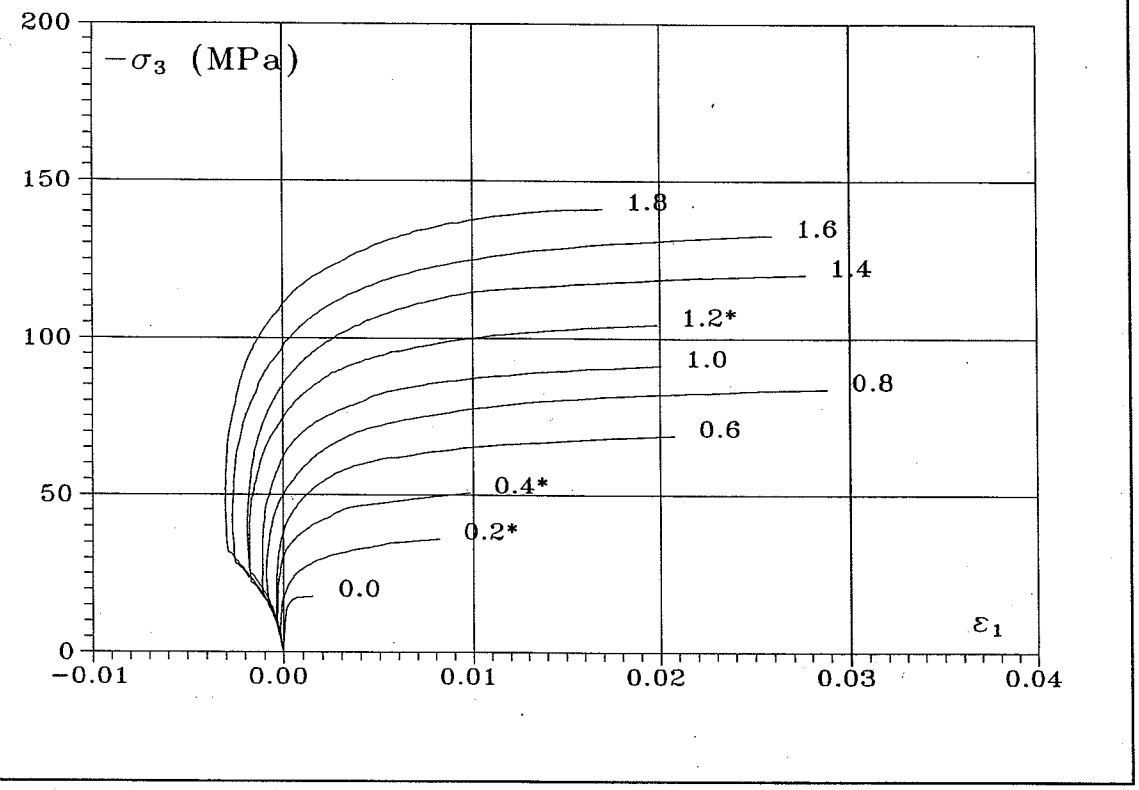

Fig. A.1.3: Major principal strain, concrete B010 - first part.

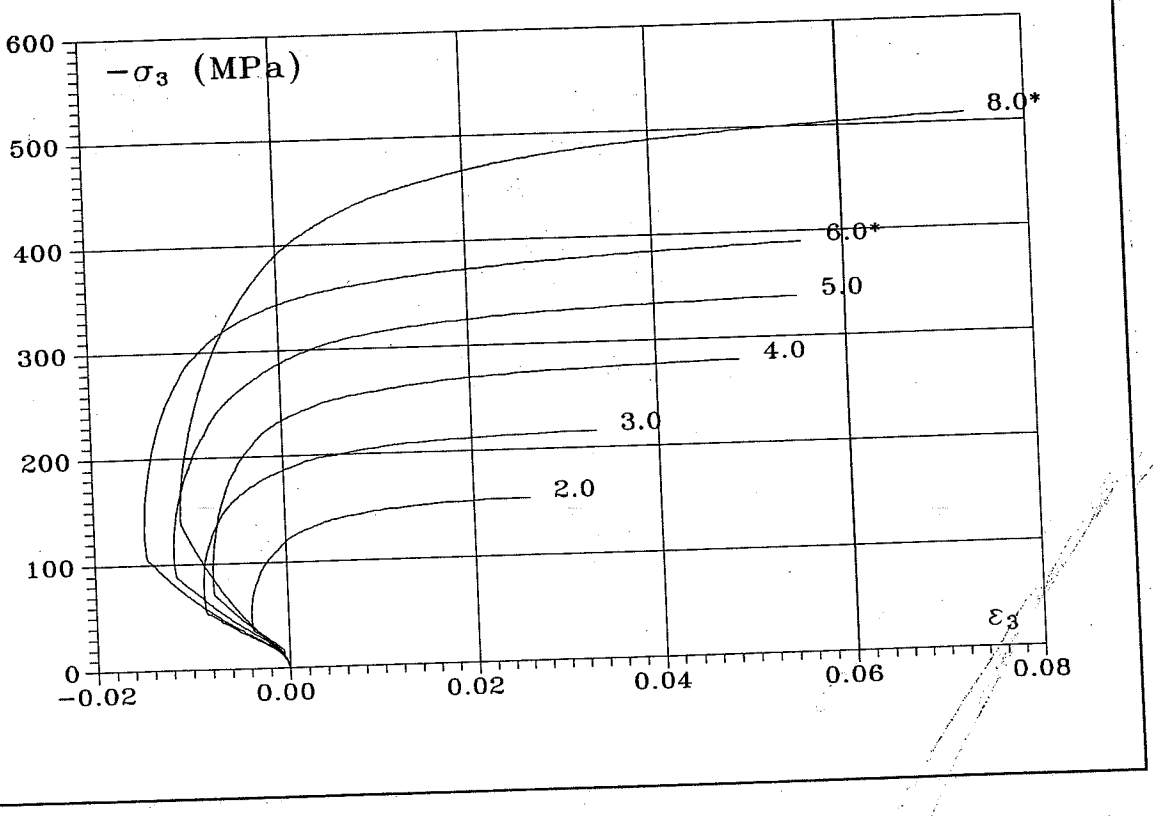

Fig. A.1.4: Major principal strain, concrete B010 - second part.

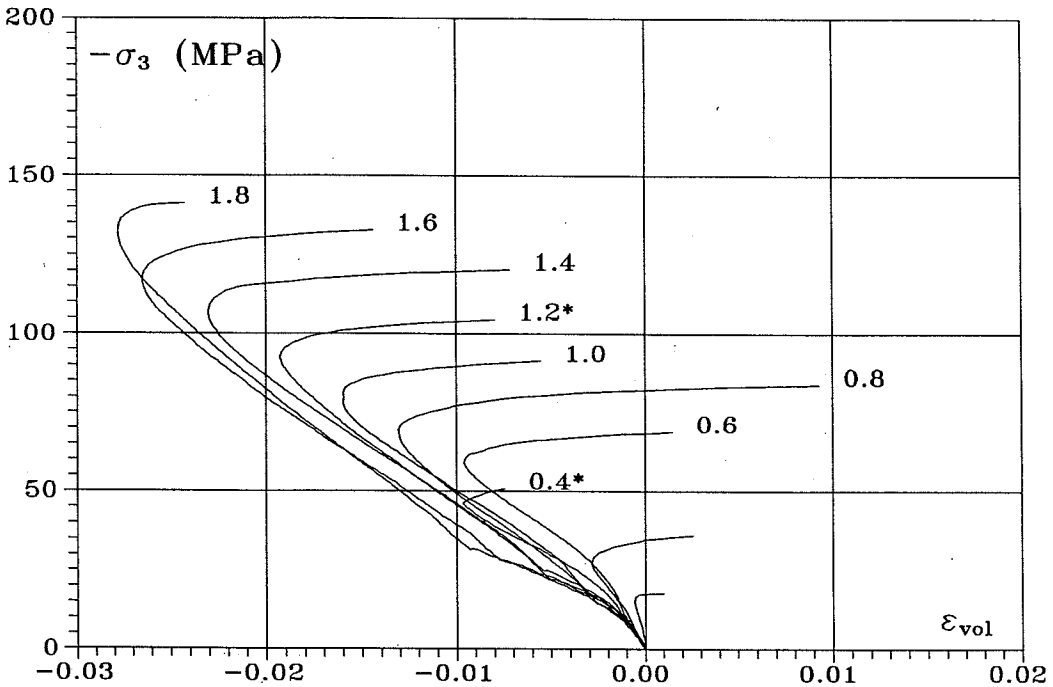

Fig. A.1.5: Volumetric strain, concrete B010 - first part.

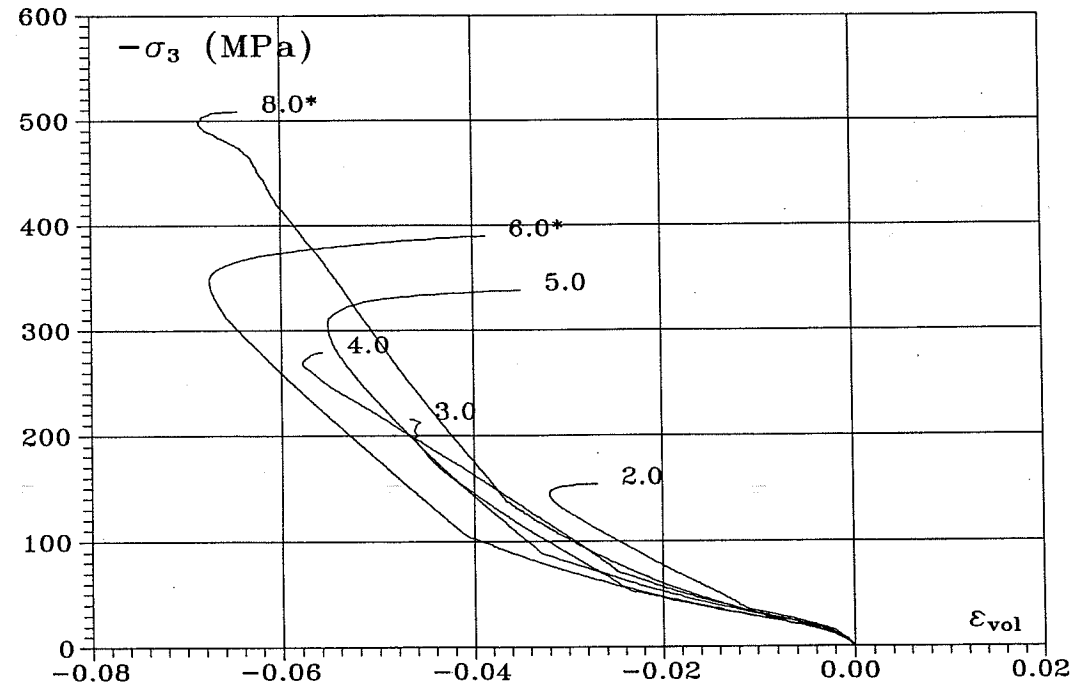

Fig. A.1.6: Volumetric strain, concrete B010 - second part.

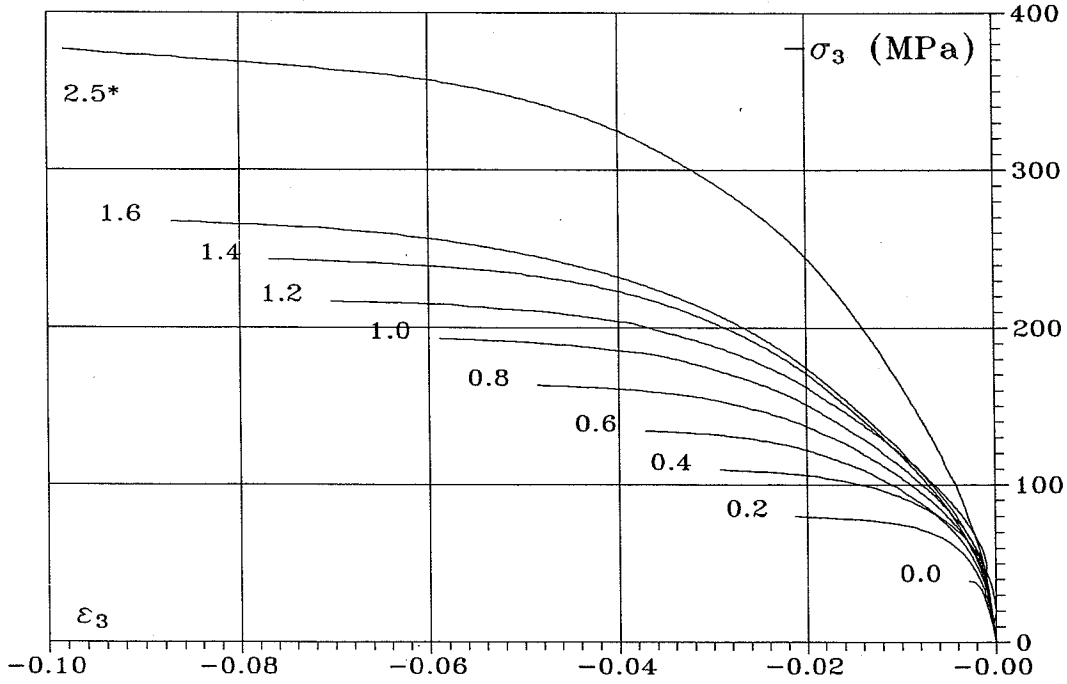

Fig. A.1.7: Minor principal strain, concrete B035.

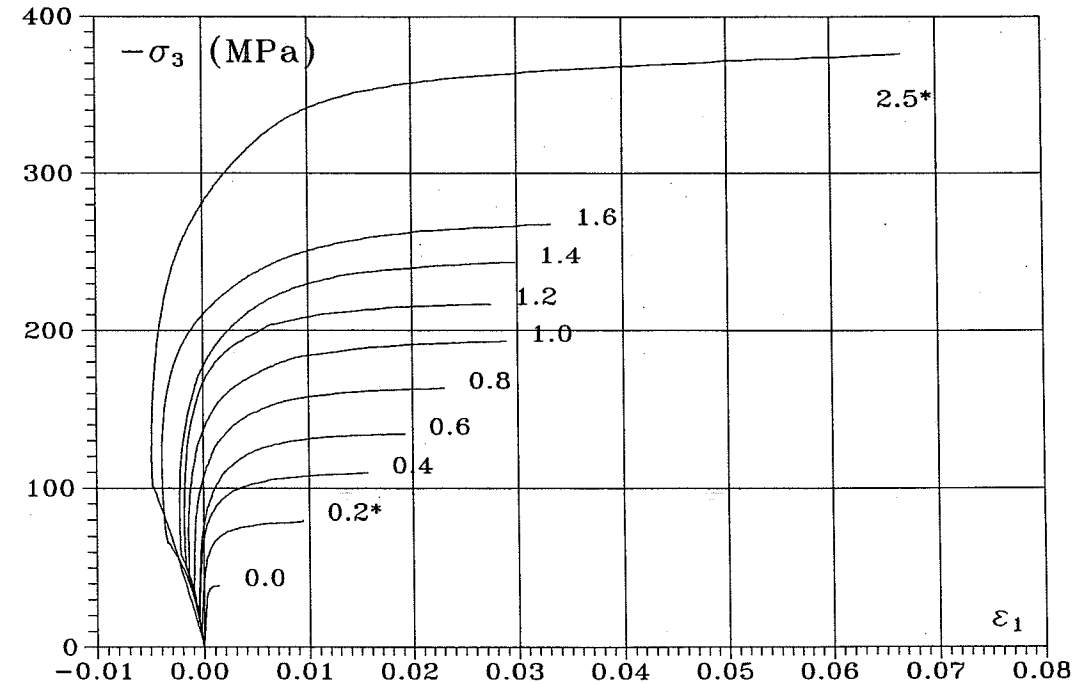

Fig. A.1.8: Major principal strain, concrete B035.

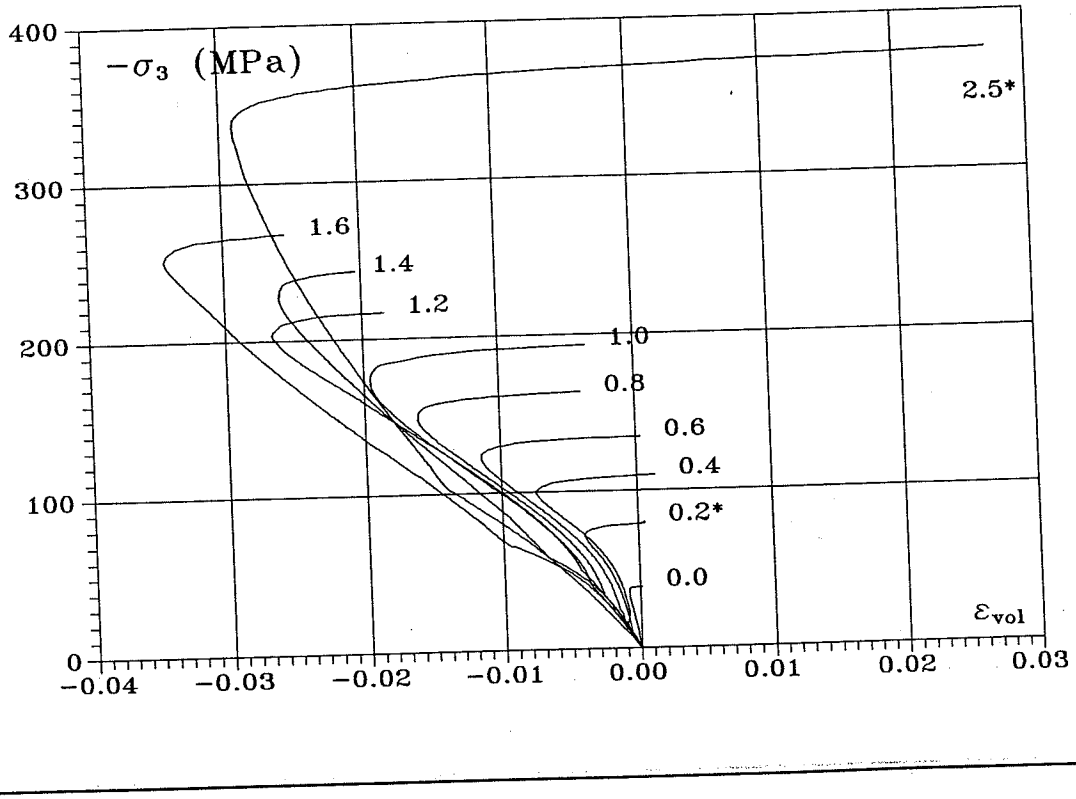

Fig. A.1.9: Volumetric strain, concrete B035.

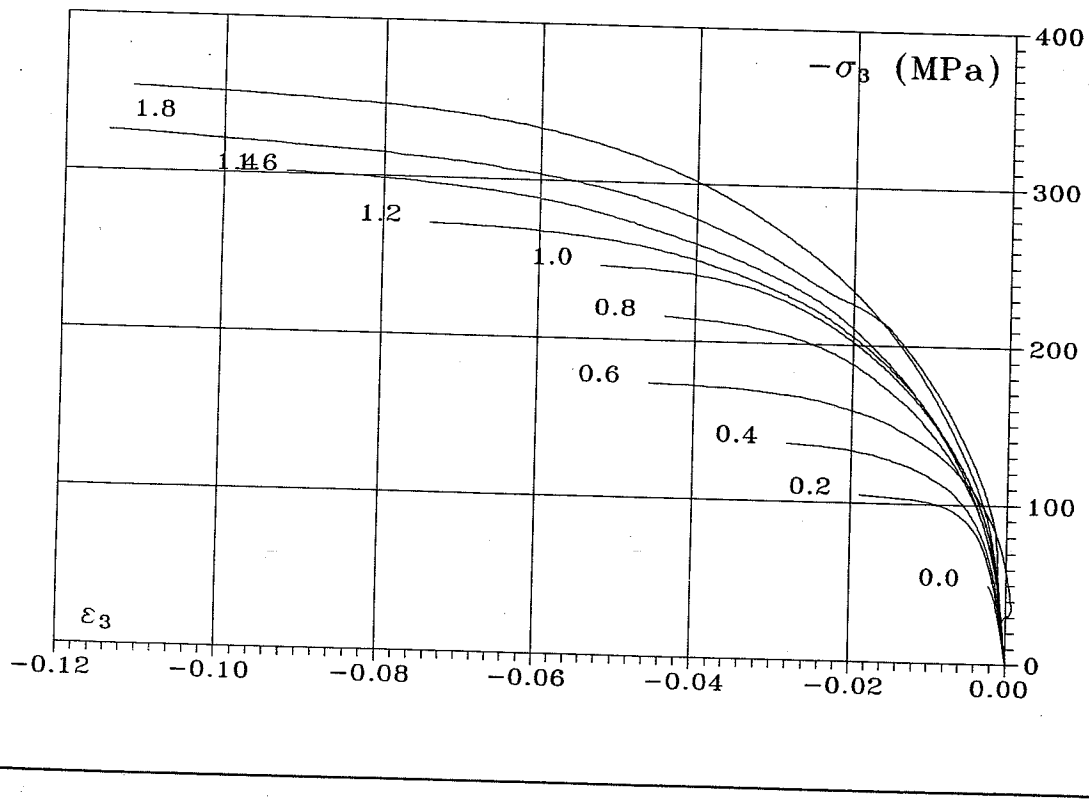

Fig. A.1.10: Minor principal strain, concrete B050.

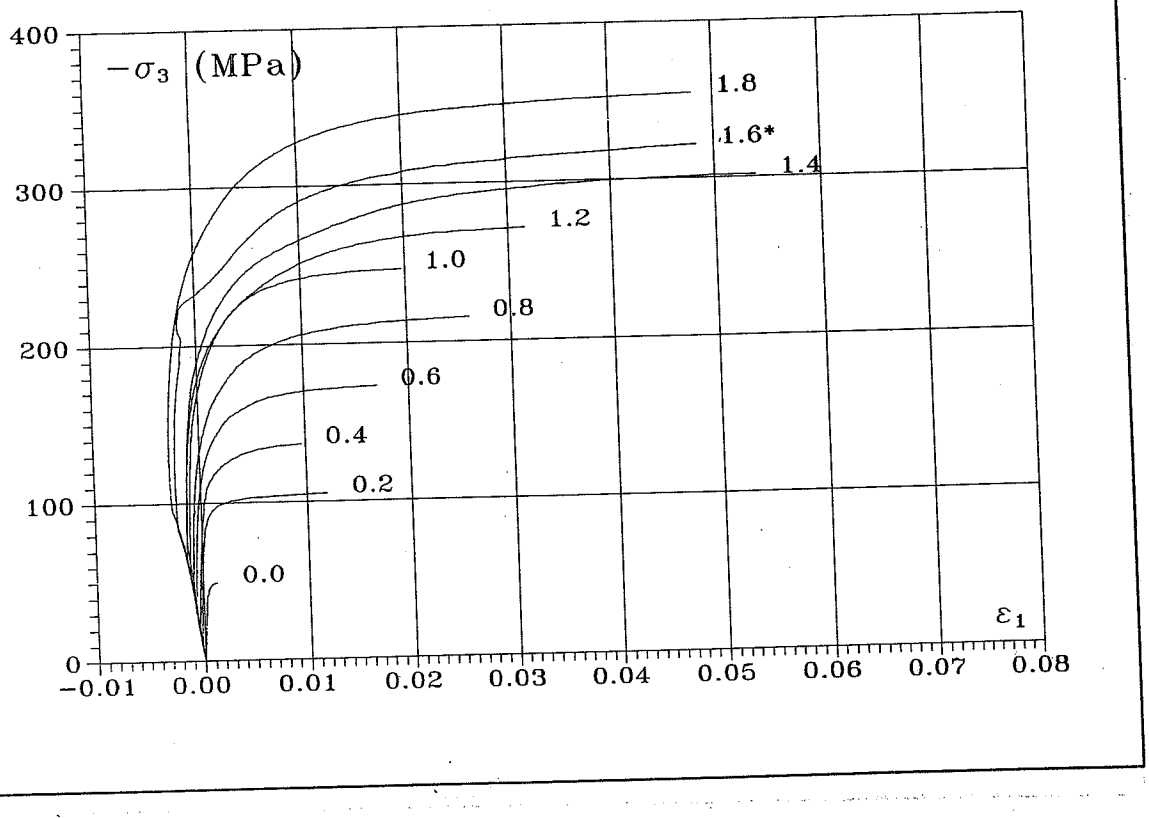

Fig. A.1.11: Major principal strain, concrete B050.

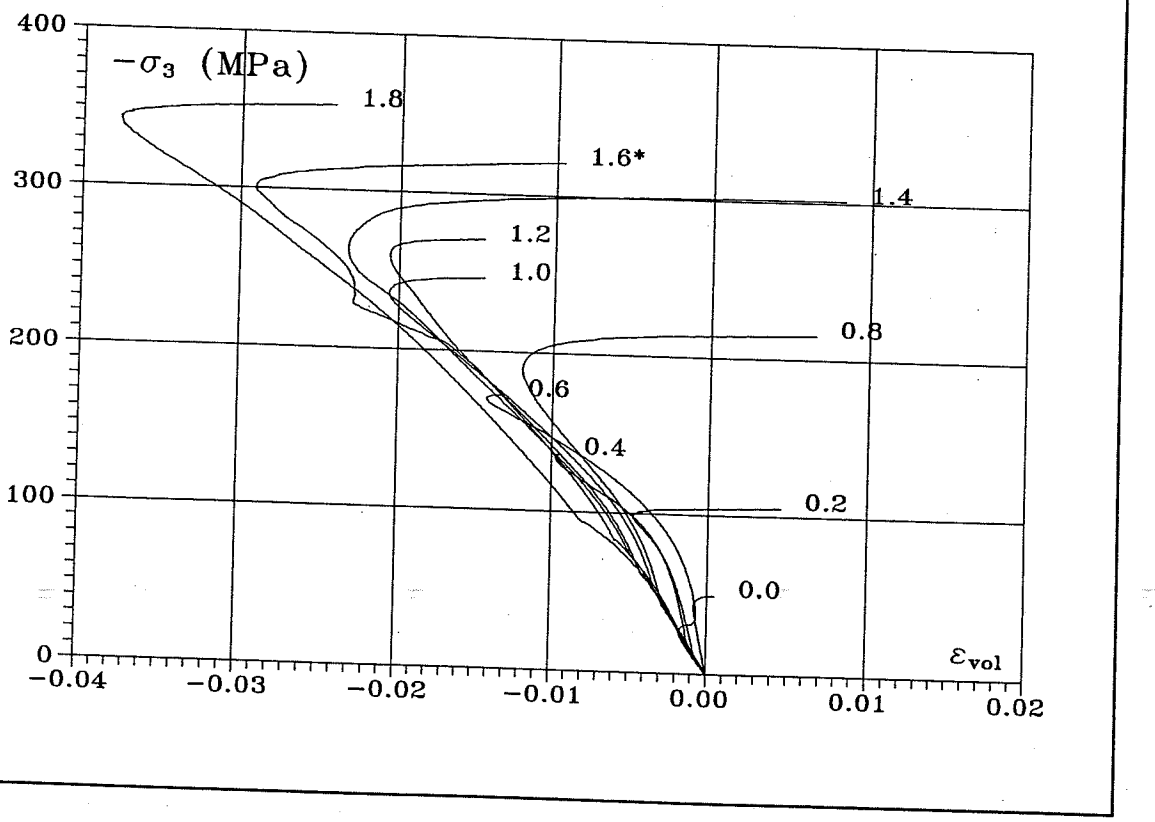

Fig. A.1.12: Volumetric strain, concrete B050.

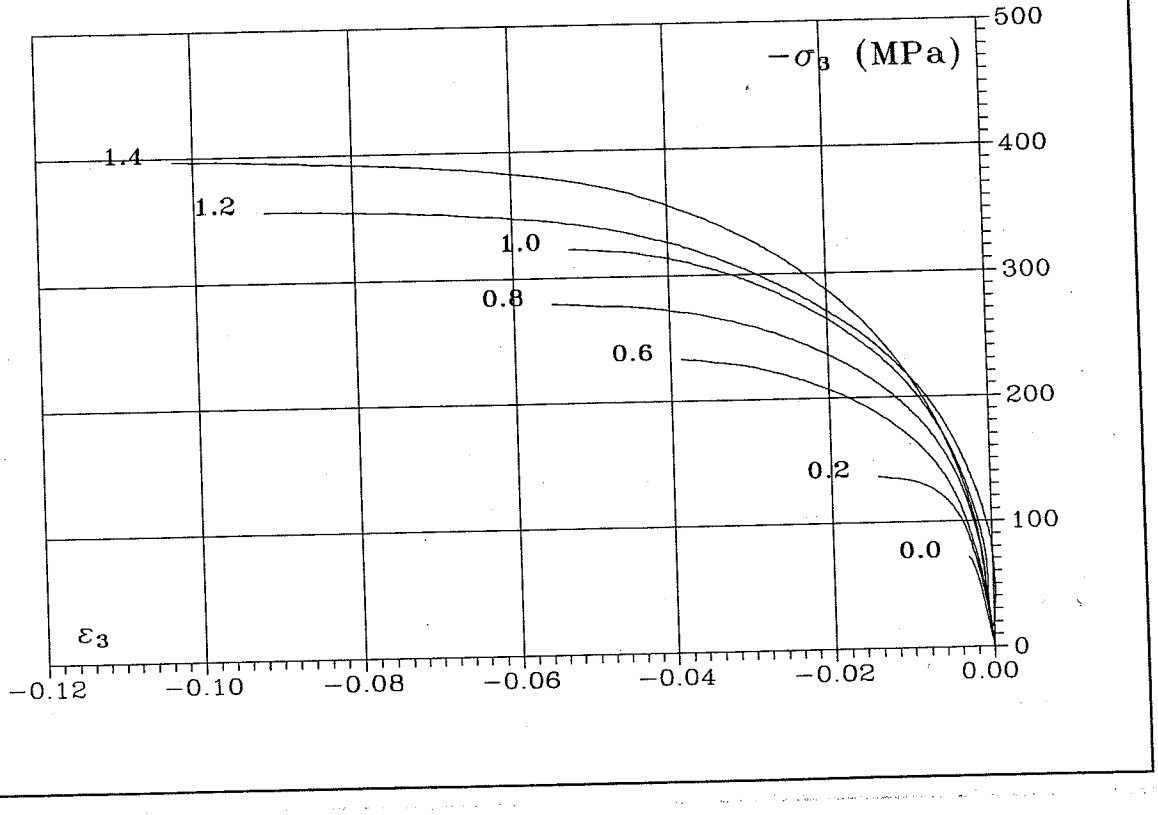

Fig. A.1.13: Minor principal strain, concrete B070.

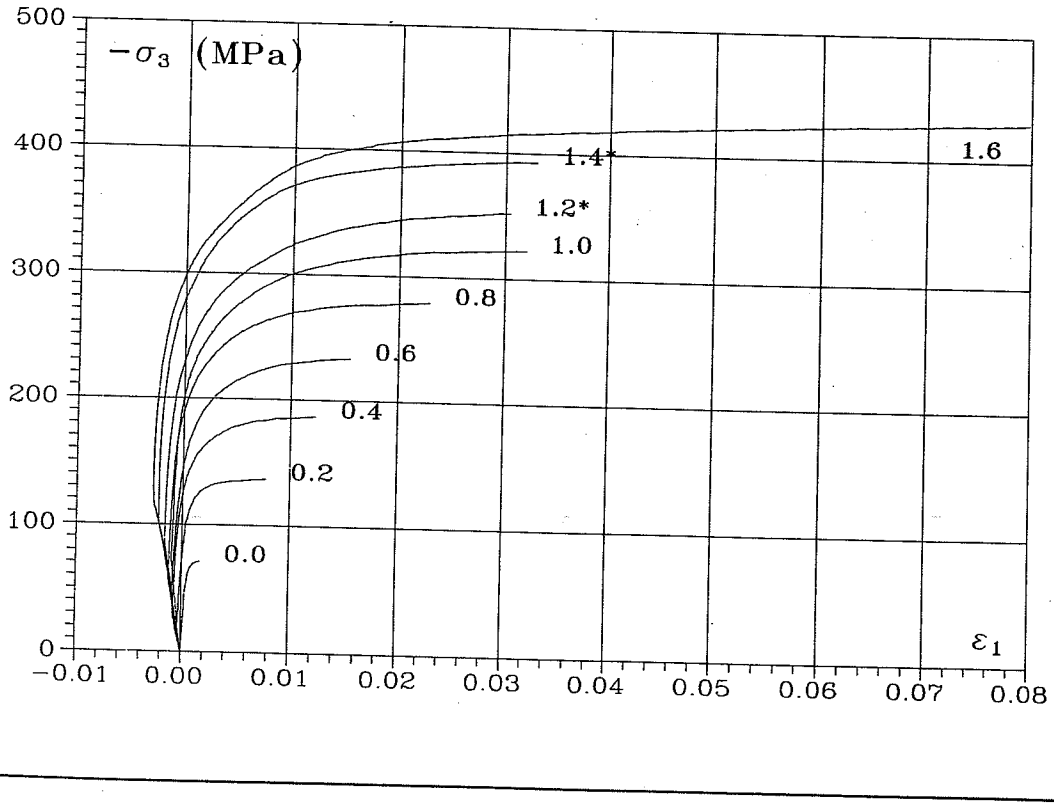

Fig. A.1.14: Major principal strain, concrete B070.

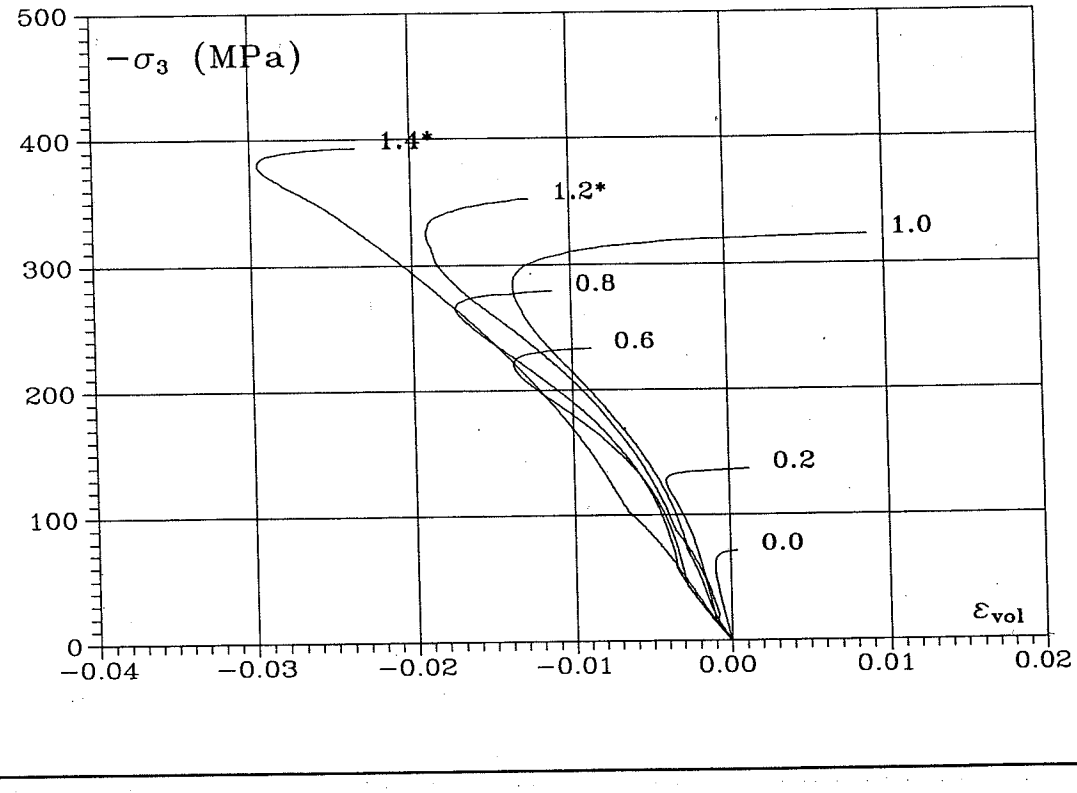

Fig. A.1.15: Volumetric strain, concrete B070.

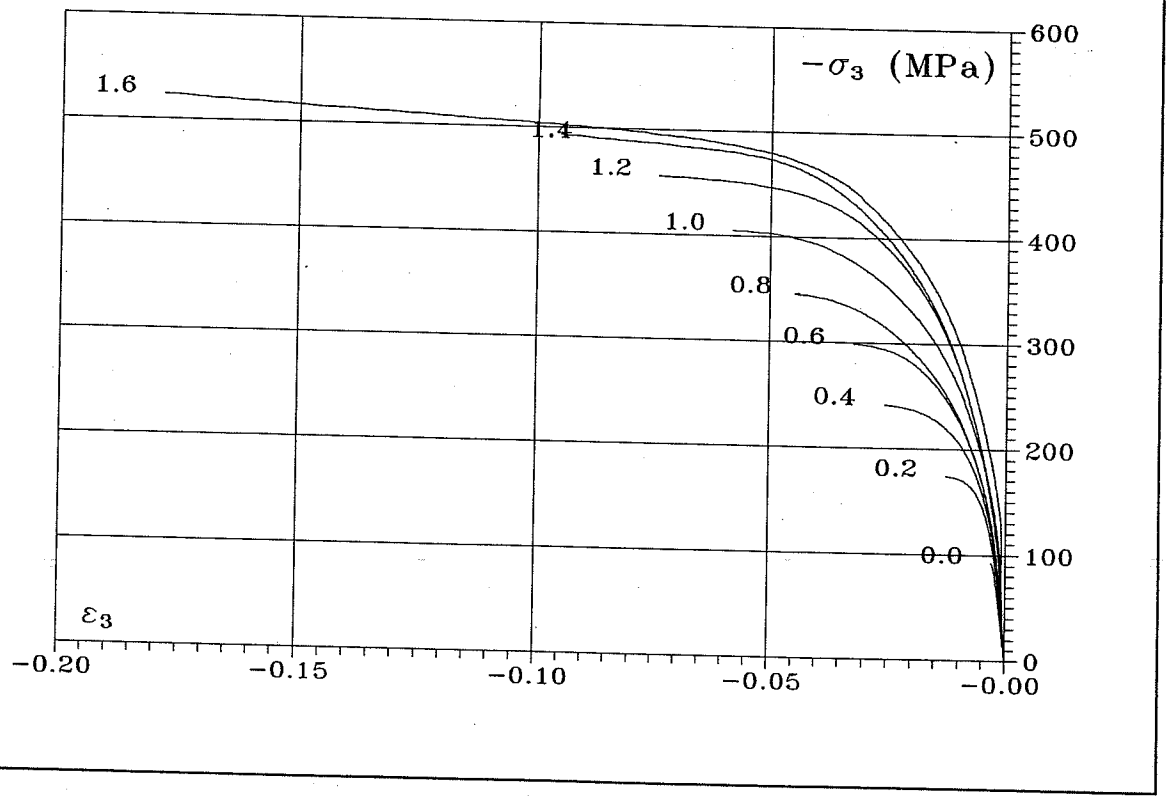

Fig. A.1.16: Minor principal strain, concrete B085.

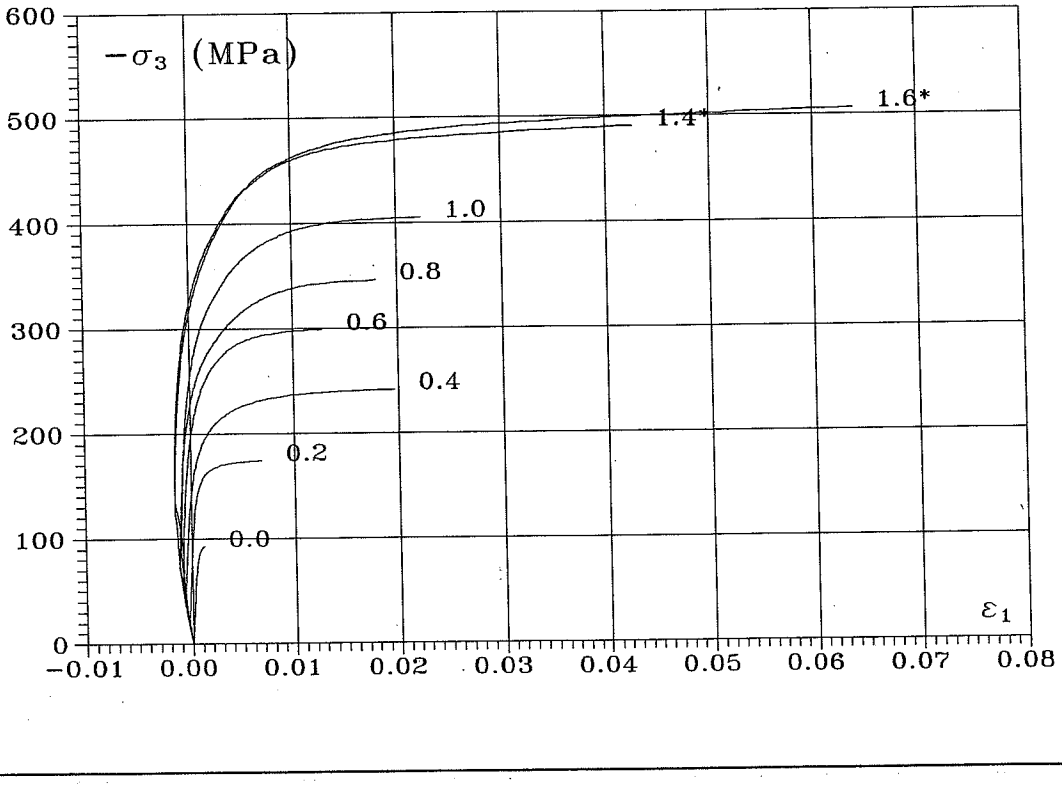

Fig. A.1.17: Major principal strain, concrete B085.

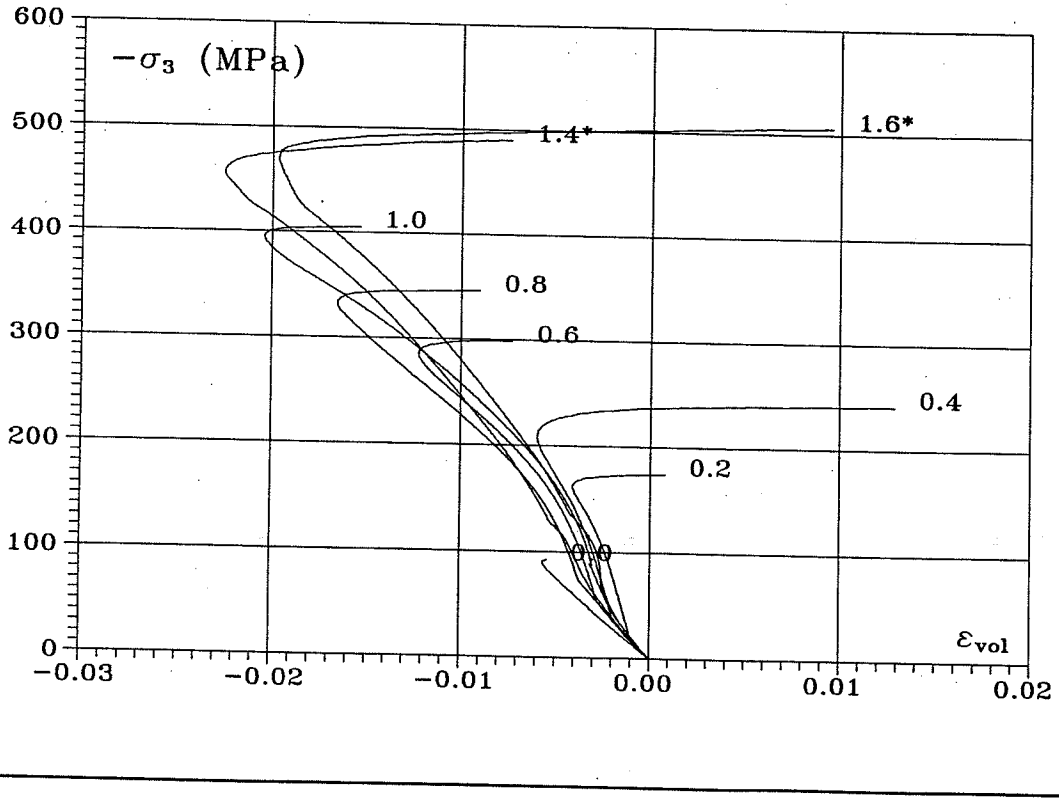

Fig. A.1.18: Volumetric strain, concrete B085.

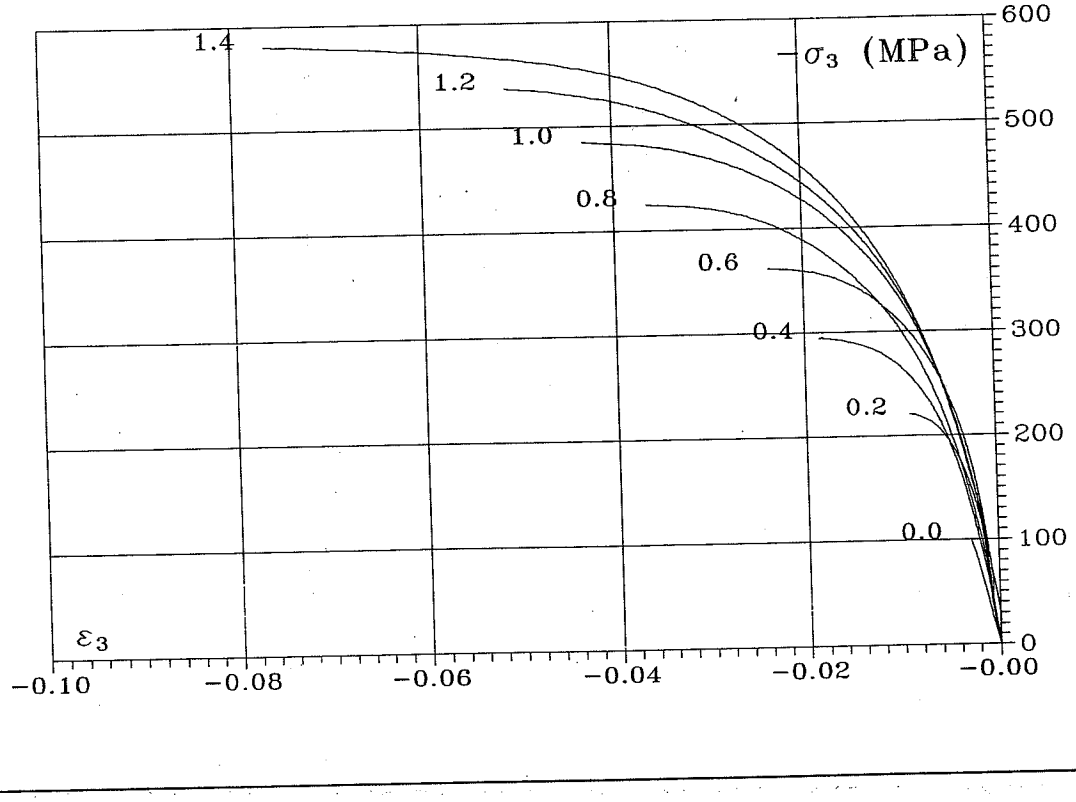

Fig. A.1.19: Minor principal strain, concrete B100.

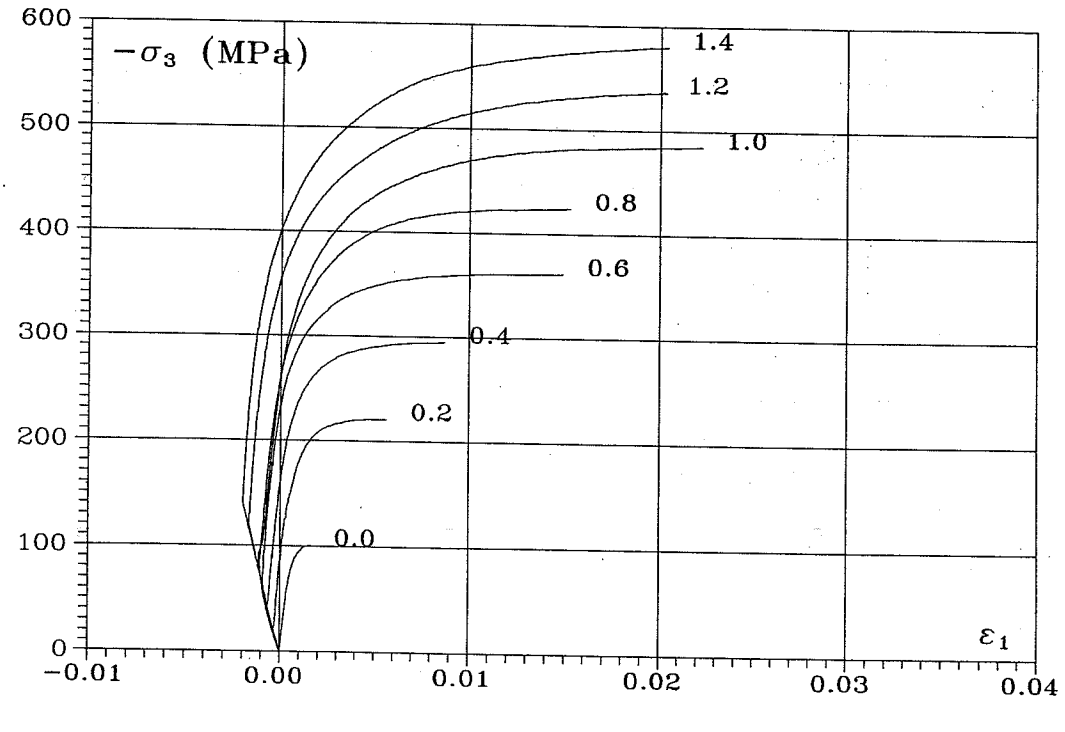

Fig. A.1.20: Major principal strain, concrete B100.

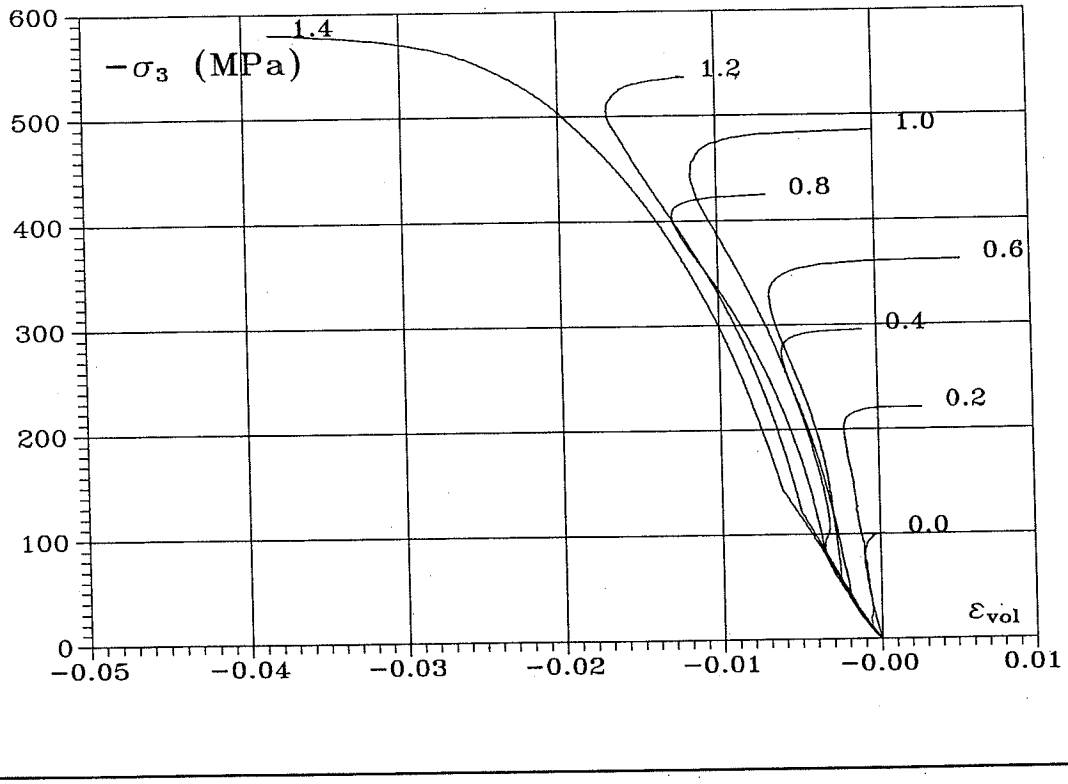

Fig. A.1.21: Volumetric strain, concrete B100.

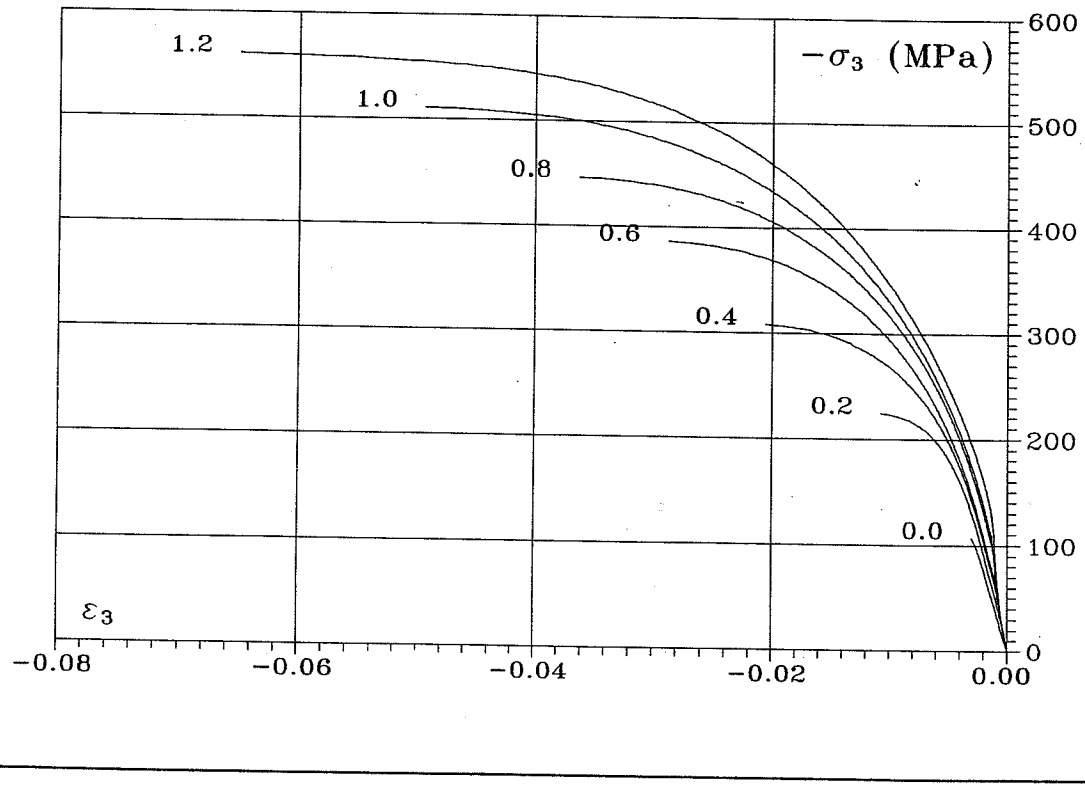

Fig. A.1.22: Minor principal strain, concrete B110.

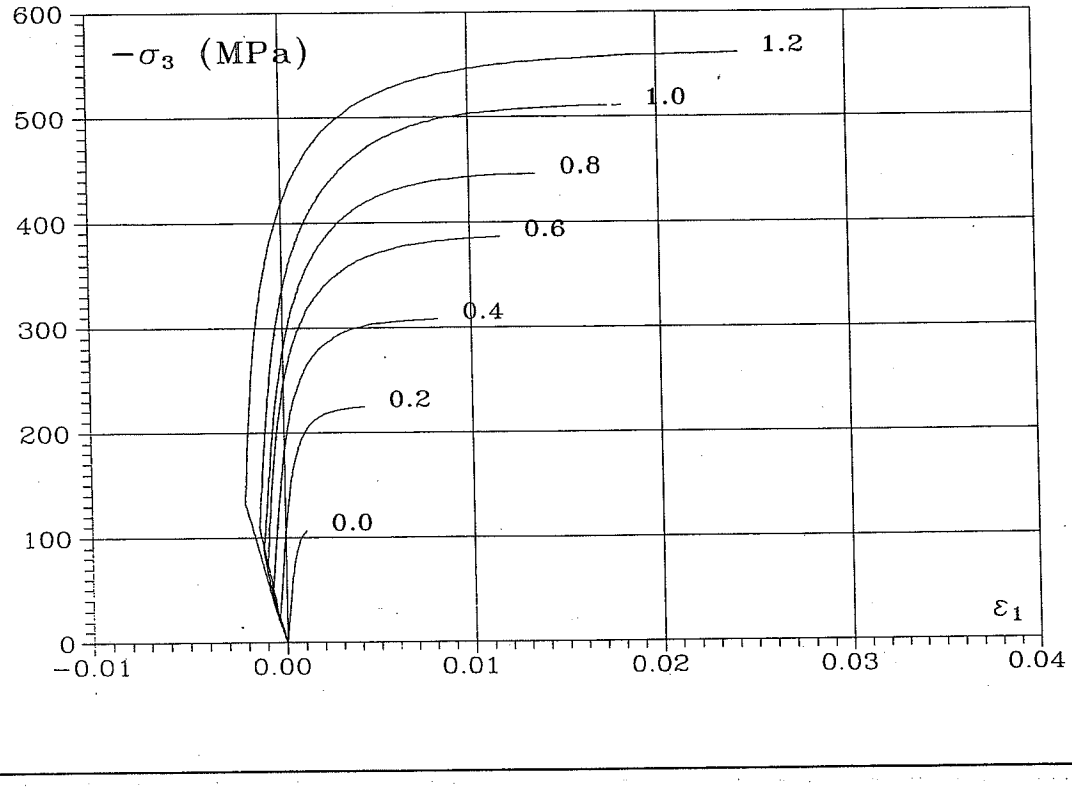

Fig. A.1.23: Major principal strain, concrete B110.

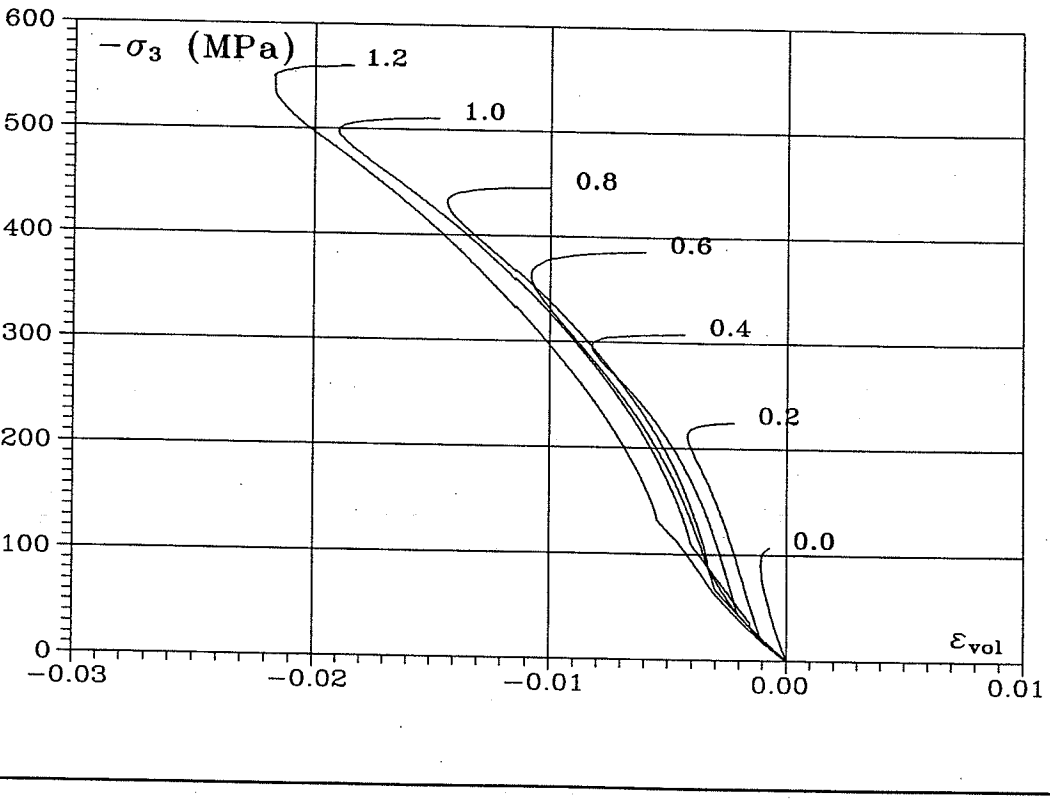

Fig. A.1.24: Volumetric strain, concrete B110.

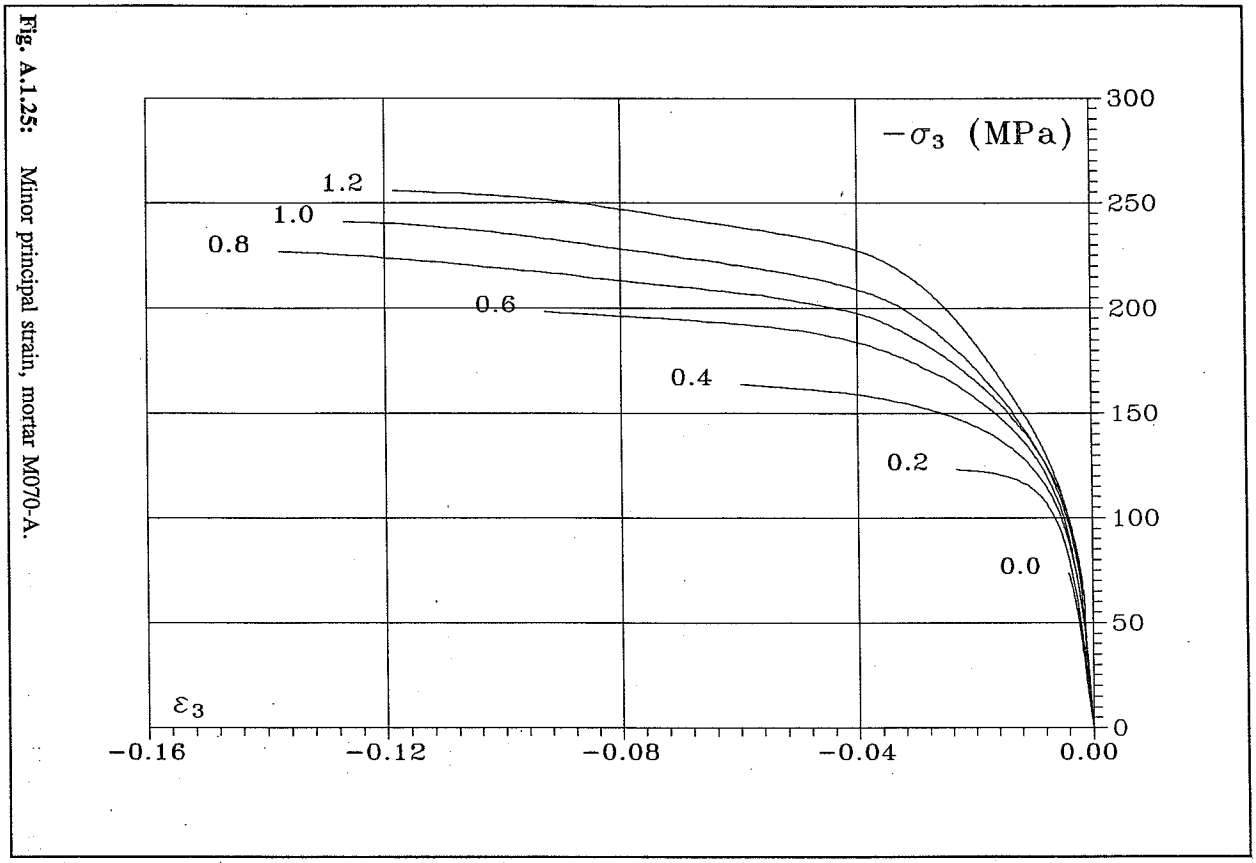

Fig. A.1.25: Minor principal strain, mortar M070-A.

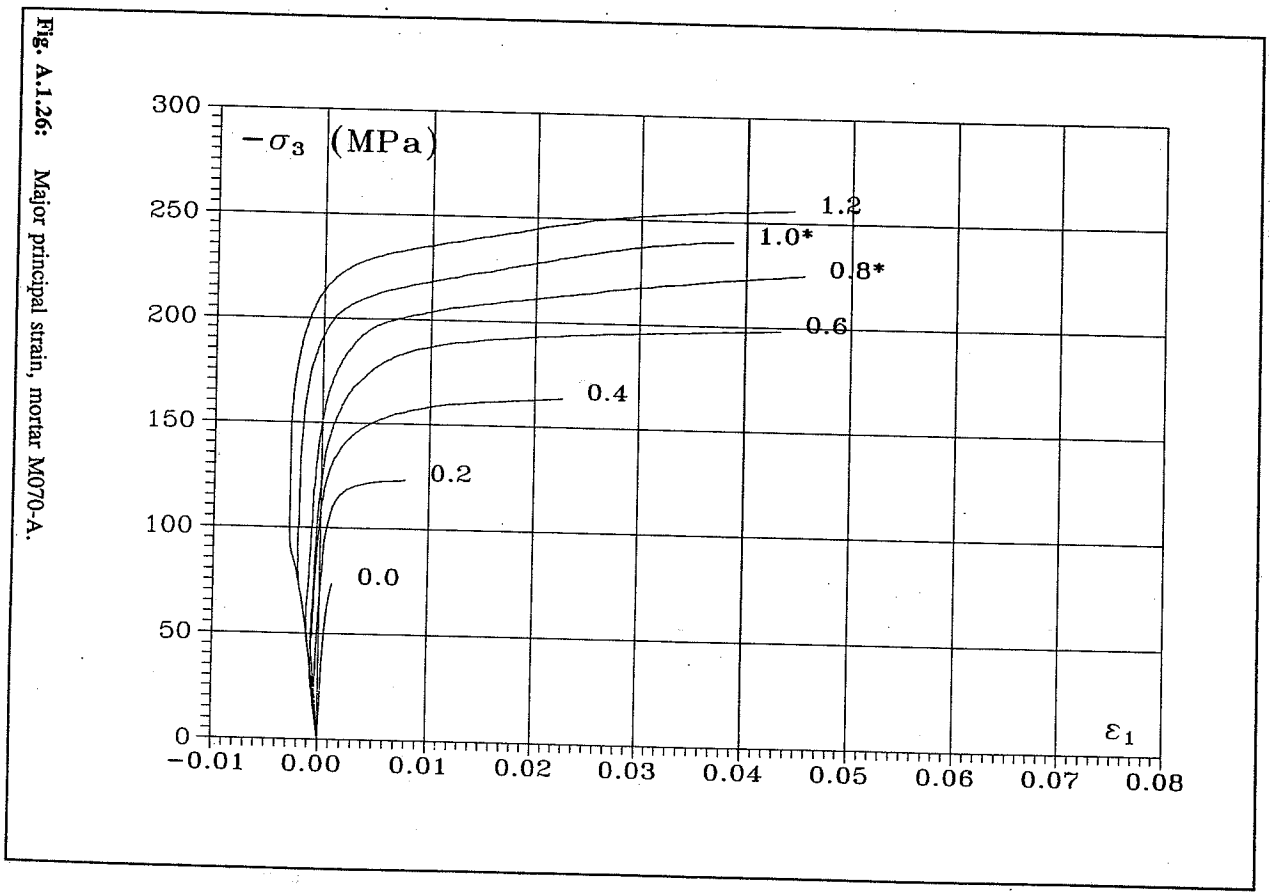

Fig. A.1.26: Major principal strain, mortar M070-A.

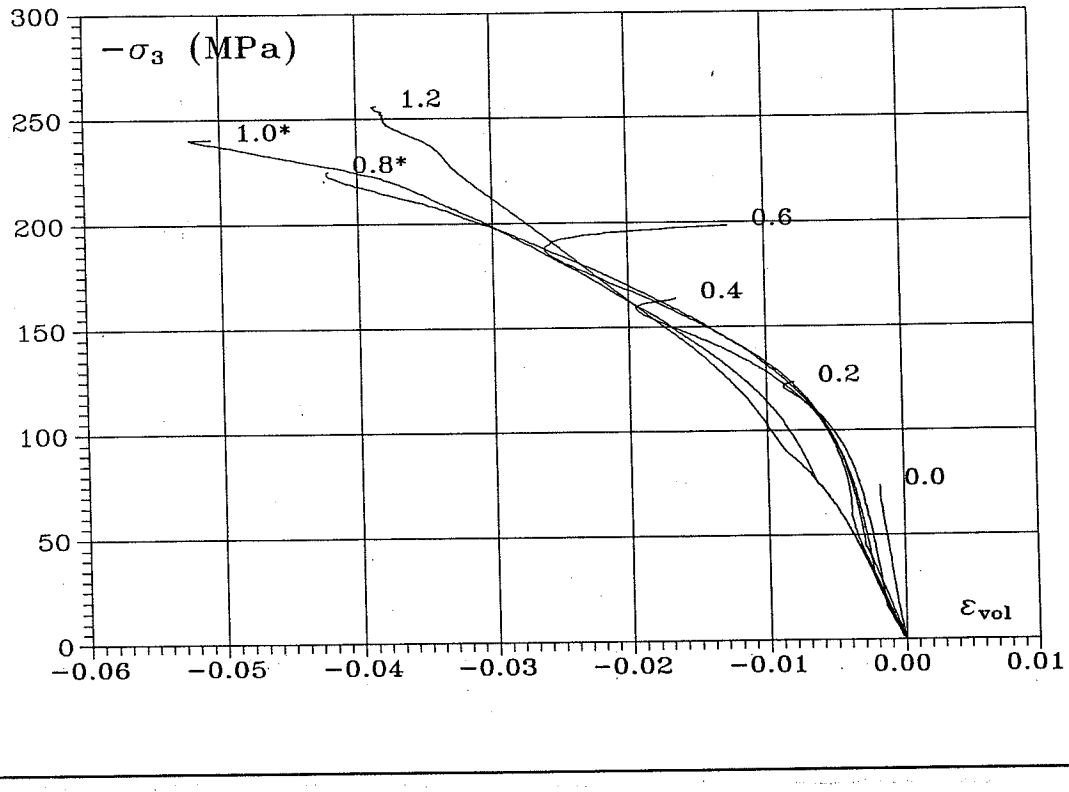

Fig. A.1.27: Volumetric strain, mortar M070-A.

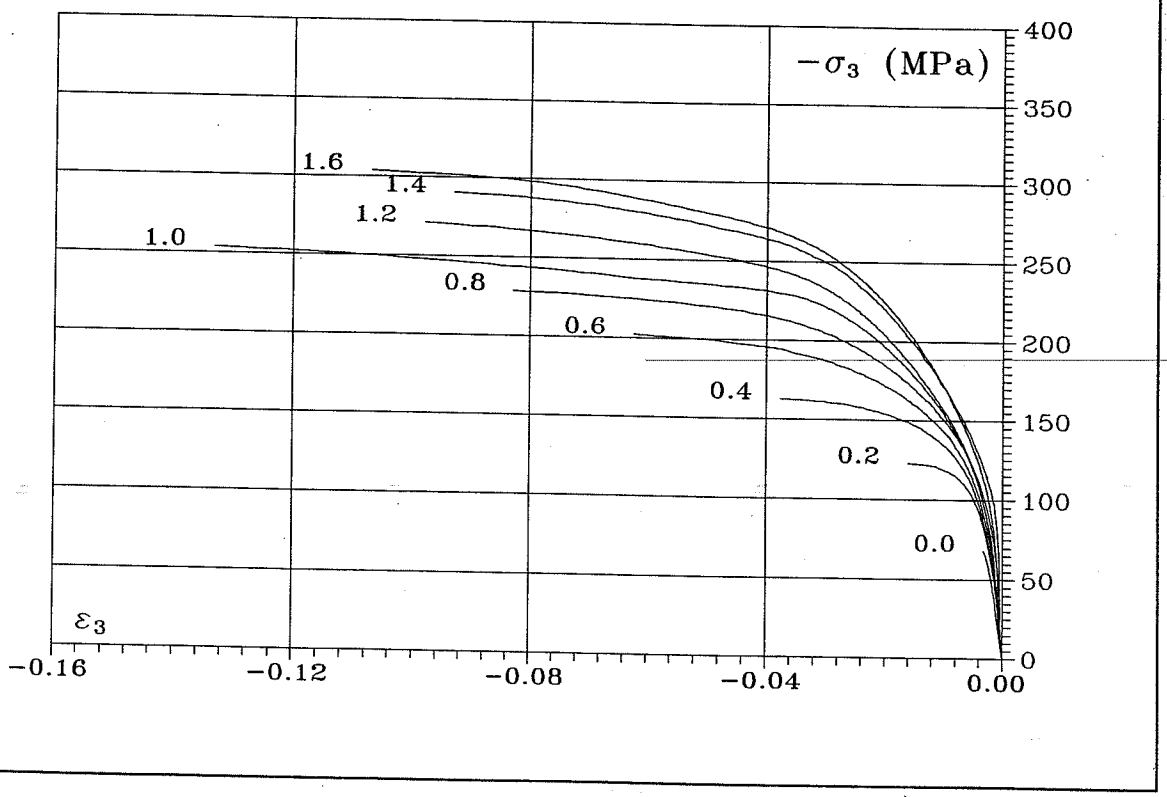

Fig. A.1.28: Minor principal strain, mortar M070-B.

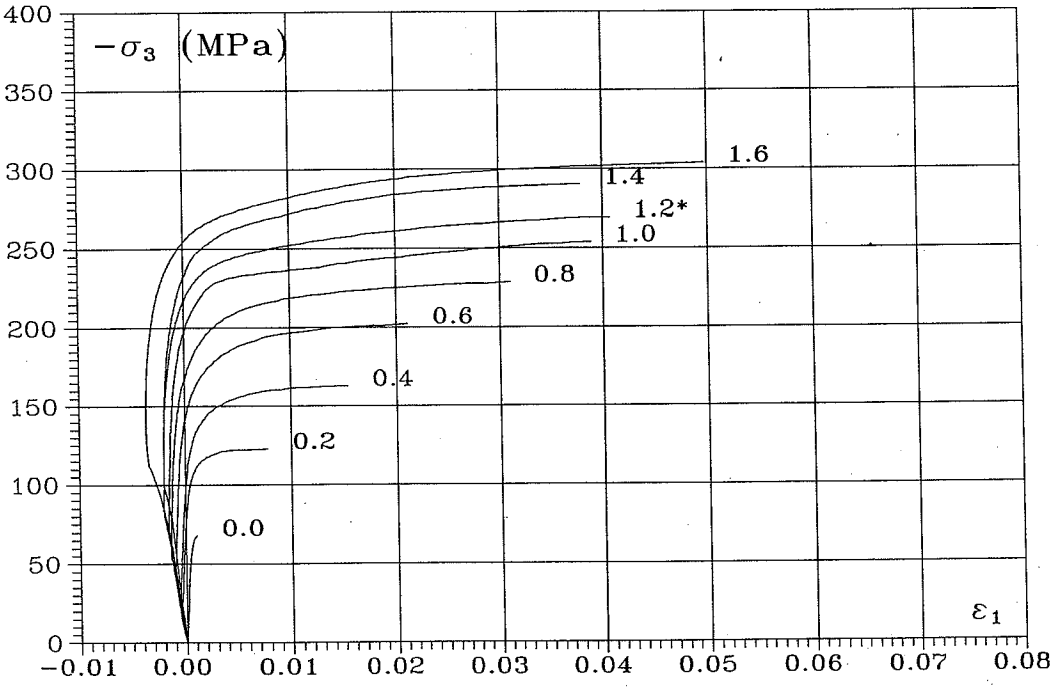

Fig. A.1.29: Major principal strain, mortar M070-B.

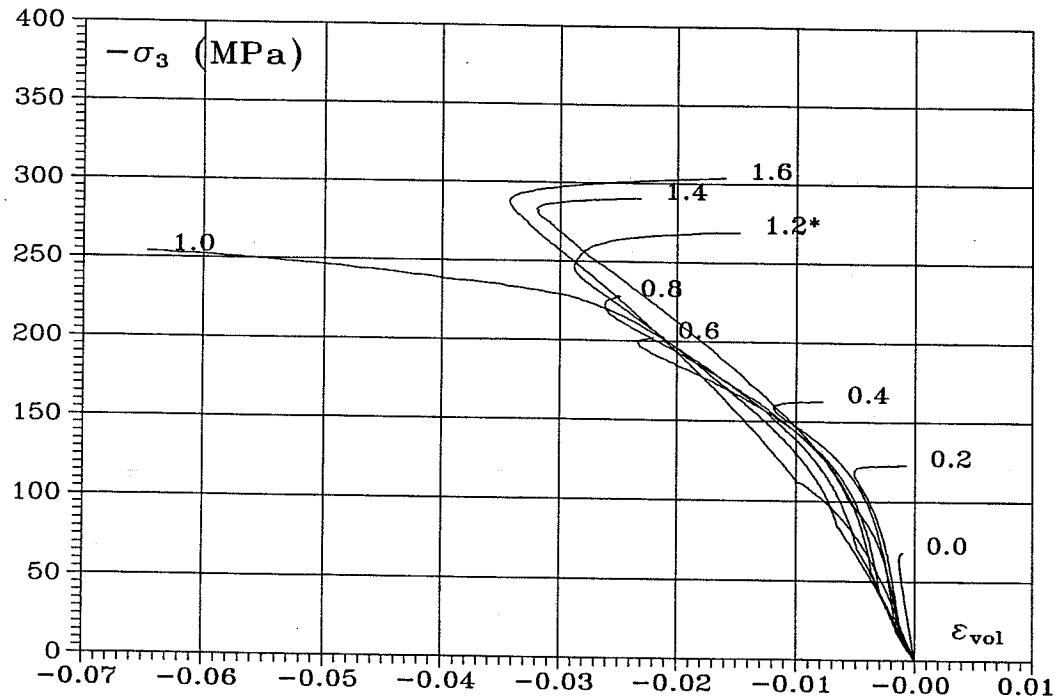

Fig. A.1.30: Volumetric strain, mortar M070-B.

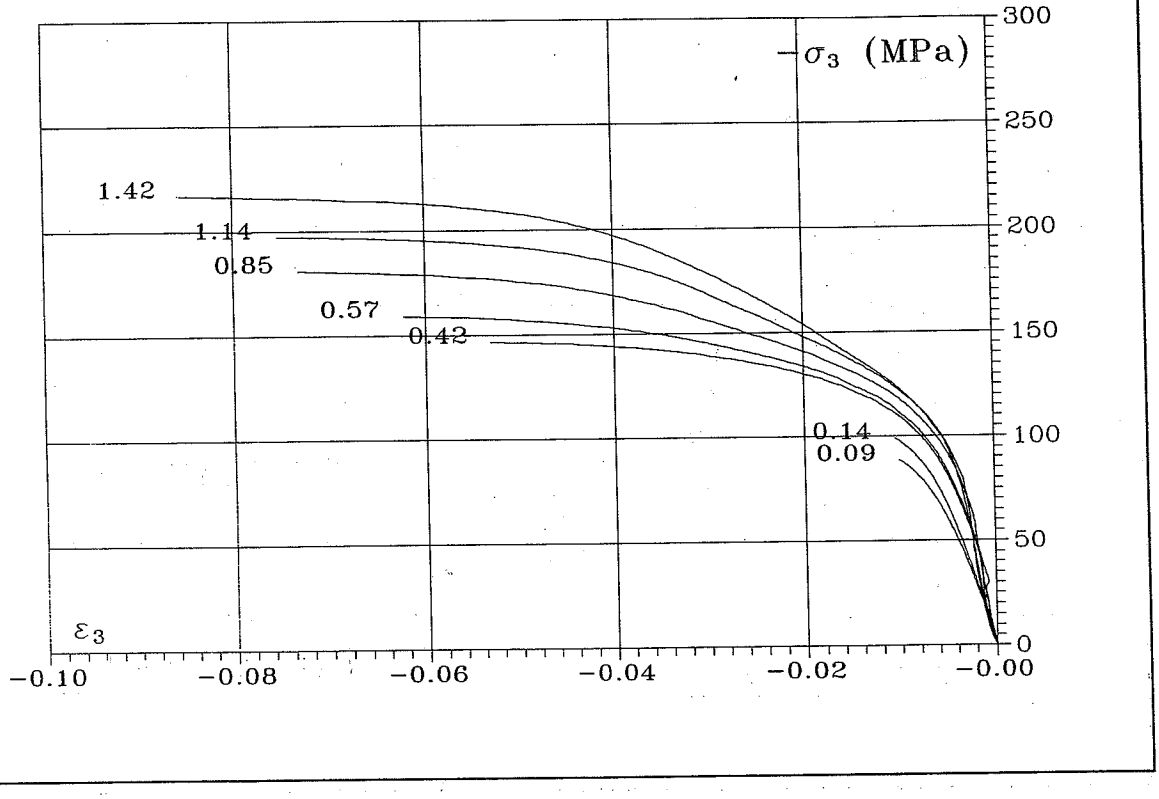

Fig. A.1.31: Minor principal strain, paste P070.

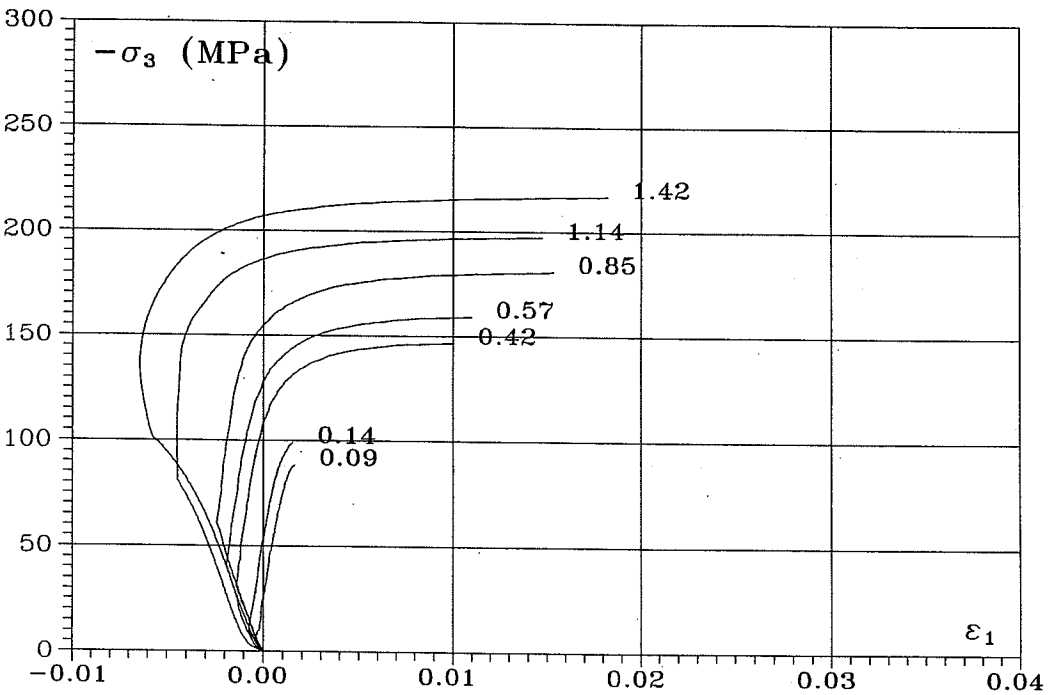

Fig. A.1.32: Major principal strain, paste P070.

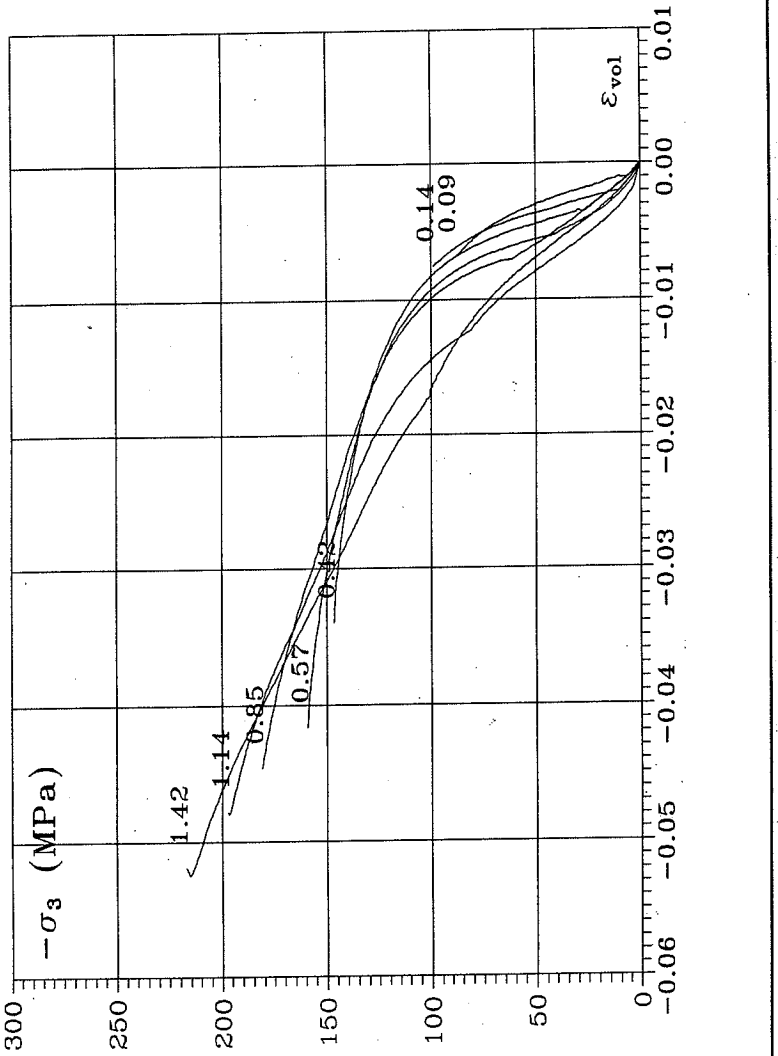

Fig. A.1.33: Volumetric strain, paste P070.

Appendix 2

Experimental results

In this appendix are given in tabular form the usable results of the test program. For each test specimen the following results are stated:

uniaxial concrete strength, f_c
minor principal stress at failure, σ_{3f}
major principal stress at failure, σ_{1f}
maximum hydrostatic strain, $\epsilon_{0,max}$
minor principal strain at failure, ϵ_{3f}
major principal strain at failure, ϵ_{1f}
initial deviatoric Young's modulus, E_i
secant value of Young's modulus at failure, E_f

Concrete B010-3, f_c= 17.08 MPa							
Specimen	σ_{3f} (MPa)	σ_{1f} (MPa)	$\epsilon_{0,max}$ (‰)	ϵ_{3f} (‰)	ϵ_{1f} (‰)	E_i (MPa)	E_f (MPa)
B010-3-00	-17.08	0.00	0.00	-2.04	-1.53	23922	8701
B010-3-01	-38.62	-4.06	-0.16	-21.97	***	16405	1587
B010-3-02	-52.93	-7.24	-0.27	-33.70	***	13205	1372
B010-3-03	-68.06	-10.66	-0.35	-38.86	-20.78	13721	1513
B010-3-04	-83.17	-14.25	-0.86	-46.45	-28.81	7721	1528
B010-3-05	-91.12	-17.53	-0.97	-44.37	-20.10	7744	1705
B010-3-06	-105.82	-20.97	-1.48	-57.37	***	6213	1527
B010-3-07	-120.14	-24.20	-1.69	-59.98	-27.70	5906	1649
B010-3-08	-132.60	-28.04	-2.64	-63.55	-25.91	6019	1720
B010-3-09	-141.64	-30.74	-2.98	-60.01	-16.98	5843	1942
B010-3-10	-153.21	-34.14	-3.33	-75.76	-26.08	5737	1655
B010-3-11	-215.53	-51.47	-7.22	-107.25	-33.38	6498	1643
B010-3-12	-278.46	-69.00	-8.32	-141.54	-48.77	6408	1577
B010-3-13	-337.65	-85.82	-10.49	-132.97	-55.05	8193	2059
B010-3-14	-397.10	-103.63	-13.33	-167.99	***	8499	1898
B010-3-15	-516.22	-138.11	-13.10	-212.53	***	9609	1894

Table A.2.1: Test results, concrete B010-3.

Note: *** denotes gauge failure.

Concrete B035-3, f_c= 40.41 MPa							
Specimen	σ_{3f} (MPa)	σ_{1f} (MPa)	$\epsilon_{0,max}$ (‰)	ϵ_{3f} (‰)	ϵ_{1f} (‰)	E_i (MPa)	E_f (MPa)
B035-3-00	-40.41	0.00	0.00	-2.75	-1.43	28900	14142
B035-3-01	-77.85	-8.47	-0.20	-21.25	***	28531	3411
B035-3-02	-109.27	-16.53	-0.29	-29.29	-15.66	***	3211
B035-3-03	-134.06	-24.26	-0.54	-37.18	-19.30	22725	3004
B035-3-04	-163.14	-32.57	-0.82	-48.52	-23.12	21341	2749
B035-3-05	-192.96	-40.79	-1.17	-58.86	-28.96	23130	2648
B035-3-06	-216.20	-48.57	-1.27	-70.29	-27.54	19542	2445
B035-3-07	-242.87	-56.89	-2.17	-76.79	-29.84	10701	2495
B035-3-08	-267.17	-64.81	-2.87	-87.18	-33.25	9478	2402
B035-3-11	-395.86	-101.13	-4.47	***	***	****	***

Table A.2.2: Test results, concrete B035-3.

Note: *** denotes gauge failure.

Concrete B050-3, f_c= 51.54 MPa							
Specimen	σ_{3f} (MPa)	σ_{1f} (MPa)	$\epsilon_{0,max}$ (‰)	ϵ_{3f} (‰)	ϵ_{1f} (‰)	E_i (MPa)	E_f (MPa)
B050-3-00	-51.54	0.00	0.00	-2.23	-1.35	33020	22233
B050-3-01	-103.53	-10.97	-0.23	-18.92	-11.89	29601	5063
B050-3-02	-136.54	-21.27	-0.43	-28.24	-9.62	30472	4155
B050-3-03	-171.96	-31.08	-0.71	-45.67	-16.92	***	3123
B050-3-04	-214.73	-41.70	-0.09	-43.86	-26.04	28034	4047
B050-3-05	-246.67	-51.87	-1.07	-52.09	-19.65	26417	3826
B050-3-06	-270.74	-61.87	-1.37	-74.15	-31.68	20930	2876
B050-3-07	-300.81	-72.16	-1.67	-92.17	-53.90	15106	2538
B050-3-08	-325.21	-82.53	-1.79	-114.59	***	18343	2155
B050-3-09	-353.67	-92.86	-2.57	-111.55	-48.01	13474	2398

Table A.2.3: Test results, concrete B050-3.

Note: *** denotes gauge failure.

Concrete B070-2, f_c= 71.65 MPa							
Specimen	σ_{3f} (MPa)	σ_{1f} (MPa)	$\epsilon_{0,max}$ (‰)	ϵ_{3f} (‰)	ϵ_{1f} (‰)	E_i (MPa)	E_f (MPa)
B070-2-00	-71.65	0.00	0.00	-2.93	-1.68	30059	24280
B070-2-01	-135.79	-14.68	-0.31	-14.14	-7.77	34888	8829
B070-2-03	-232.62	-43.73	-0.94	-38.70	-15.44	30762	5001
B070-2-04	-278.46	-57.86	-1.10	-55.10	-22.96	43421	4094
B070-2-05	-321.92	-72.02	-0.90	-52.69	-32.04	34925	4850
B070-2-07	-397.01	-100.27	-2.10	-102.54	***	21870	2955

Table A.2.4: Test results, concrete B070-2.

Note: *** denotes gauge failure.

Concrete B085-3, f_c= 88.39 MPa							
Specimen	σ_{3f} (MPa)	σ_{1f} (MPa)	$\epsilon_{0,max}$ (‰)	ϵ_{3f} (‰)	ϵ_{1f} (‰)	E_i (MPa)	E_f (MPa)
B085-3-00	-88.39	0.00	0.00	-3.01	-1.19	34633	30757
B085-3-01	-173.30	-18.11	-0.33	-12.74	-6.82	36926	12533
B085-3-02	-240.61	-36.09	-0.62	-25.75	-19.63	40165	8171
B085-3-03	-298.13	-53.42	-0.90	-32.22	-12.78	37521	7831
B085-3-04	-345.22	-71.11	-1.21	-43.74	-17.99	34398	6465
B085-3-05	-405.02	-88.72	-1.02	-58.02	-22.39	40430	5568
B085-3-07	-492.97	-123.78	-1.74	-94.45	***	25877	3986
B085-3-08	-523.16	-133.03	-1.28	-178.55	***	29286	2204

Table A.2.5: Test results, concrete B085-3.

Note: *** denotes gauge failure.

Concrete B100-3, f_c= 99.82 MPa							
Specimen	σ_{3f} (MPa)	σ_{1f} (MPa)	$\epsilon_{0,max}$ (‰)	ϵ_{3f} (‰)	ϵ_{1f} (‰)	E_i (MPa)	E_f (MPa)
B100-3-00	-99.82	0.00	0.00	-2.90	-1.58	40983	34707
B100-3-02	-294.43	-40.40	-0.62	-18.08	-8.7	44667	14569
B100-3-03	-360.69	-60.39	-0.80	-23.71	-14.87	***	13138
B100-3-04	-424.32	-80.12	-1.20	-36.48	-15.25	44097	9749
B100-3-05	-484.05	-100.29	-1.15	-43.07	-22.23	***	9179
B100-3-06	-536.98	-120.09	-1.64	-51.01	-20.12	41038	8438
B100-3-07	-579.69	-139.71	-2.03	-76.36	-20.38	35214	5919

Table A.2.6: Test results, concrete B100-3.

Note: *** denotes gauge failure.

Concrete B110-2, f_c= 108.76 MPa							
Specimen	σ_{3f} (MPa)	σ_{1f} (MPa)	$\epsilon_{0,max}$ (‰)	ϵ_{3f} (‰)	ϵ_{1f} (‰)	E_i (MPa)	E_f (MPa)
B110-2-00	-108.76	0.00	0.00	-2.99	-1.13	38365	35629
B110-2-01	-224.02	-22.21	-0.36	-10.74	-4.28	41688	19469
B110-2-02	-307.01	-44.01	-0.68	-20.56	-8.25	46742	13285
B110-2-03	-385.17	-65.83	-1.00	-28.70	-11.61	44570	11562
B110-2-04	-445.97	-87.25	-1.09	-36.24	-13.52	47702	10216
B110-2-05	-510.36	-109.19	-1.34	-49.45	-18.12	42950	8340
B110-2-06	-560.04	-131.05	-1.69	-64.95	-24.33	43293	6785

Table A.2.7: Test results, concrete B110-2.

Note: *** denotes gauge failure.

Mortar M070-A, f_c= 73.49 MPa							
Specimen	σ_{3f} (MPa)	σ_{1f} (MPa)	$\epsilon_{0,max}$ (‰)	ϵ_{3f} (‰)	ϵ_{1f} (‰)	E_i (MPa)	E_f (MPa)
M070-A-00	-73.49	0.00	0.00	-3.99	-1.13	21134	18419
M070-A-01	-122.48	-14.94	-0.48	-23.21	-7.77	23358	6128
M070-A-02	-163.36	-29.72	-0.75	-59.70	-22.72	26593	2267
M070-A-03	-198.00	-44.19	-1.15	-93.01	***	23242	1674
M070-A-05	-240.79	-73.87	-2.18	-126.83	***	14970	1339
M070-A-06	-255.70	-88.46	-2.84	-118.66	-44.50	22865	1444

Table A.2.8: Test results, mortar M070-A.

Note: *** denotes gauge failure.

Mortar M070-B, f_c= 69.61 MPa							
Specimen	σ_{3f} (MPa)	σ_{1f} (MPa)	$\epsilon_{0,max}$ (‰)	ϵ_{3f} (‰)	ϵ_{1f} (‰)	E_i (MPa)	E_f (MPa)
M070-B-00	-69.61	0.00	0.00	-3.22	-1.08	25848	21618
M070-B-01	-122.71	-14.05	-0.35	-16.13	-7.79	29691	6886
M070-B-02	-162.36	-27.97	-0.62	-37.57	-15.34	29062	3637
M070-B-03	-201.79	-42.06	-0.97	-62.19	-21.20	26240	2609
M070-B-04	-228.47	-55.83	-1.14	-82.94	-31.02	27642	2111
M070-B-05	-253.77	-69.67	-1.65	-133.31	-38.87	19391	1398
M070-B-06	-270.60	-83.50	-2.23	-98.13	***	14634	1951
M070-B-07	-290.28	-97.38	-1.64	-93.13	-37.89	14313	2108
M070-B-08	-303.60	-111.66	-3.13	-107.07	-49.76	10483	1847

Table A.2.9: Test results, mortar M070-B.

Note: *** denotes gauge failure.

AFDELINGEN FOR BÆRENDE KONSTRUKTIONER
DANMARKS TEKNISKE HØJSKOLE

Department of Structural Engineering
Technical University of Denmark, DK–2800 Lyngby

SERIE R
(Tidligere: Rapporter)

R 271. VILMANN, OLE: A Harmonic Half–Space Fundamental Solution. 1991.
R 272. VILMANN, OLE: The Boundary Element Method applied in Mindlin Plate Bending Analysis. 1991.
R 273. GANWAY, CHEN, ANDREASEN, B.S., NIELSEN, M.P.: Membrane Actions Tests of Reinforced Concrete Square Slabs. 1991.
R 274. THOUGÅRD PEDERSEN, NIELS, AGERSKOV, H.: Fatigue Life Production of Offshore Steel Structures under Stochastic Loading. 1991.
R 275. ANDREASEN, B.S., NIELSEN, M.P.: Arch Effect in Reinforced Concrete one–way Slabs. 1991.
R 276. ASKEGAARD, VAGN: Prediction of Initial Crack Location in Welded Fatigue Test Specimens by the Thermoelastic Stress Analysis Technique. 1991.
R 277. NIELSEN, KARSTEN: Analyse af Skråstagsbroers egenvægtstilstand, 1991.
R 278. NIELSEN, LEIF OTTO: Continuummechanical Lagrangian finite elements. 1991.
R 279. RIBERHOLT, H.: Limtræ af dansk træ, HQL–planker, Del 2.
R 280. RIBERHOLT, H., ENQUIST, B., GUSTAFSSON, P.J., JENSEN, RALPH BO: Timber beams notches at the support, December 1991.
R 281. RIBERHOLT, H., JOHANNESEN, JOHANNES M.: Fingerskarrede rammehjørner i limtræ. 1992.
R 282. DAHL, KAARE K.B.: Uniaxial Stress–Strain Curves for Normal and High Strength Concrete. 1992.
R 283. DULEVSKI, DAVID ENCHO: Global Structural Analysis of Steel Box Girder Bridges. 1992.
R 284. Resumeoversigt 1991 – Summaries of Papers 1991.
R 285. DAHL, KAARE K.B.: The Calibration and Use of a Triaxial Cell. 1992.
R 286. DAHL, KAARE K.B.: A Failure Criterion for Normal and High Strength Concrete. 1992.
R 287. DAHL, KAARE K.B.: A Constitutive Model for Normal and High Strength Concrete. 1992.
R 288. JENSEN, HENRIK ELGAARD: State–of–the–ark Rapport for Højstyrkebetons Svind og Krybning. 1992.
R 289. JENSEN, HENRIK ELGAARD: Creep and Shrinkage of High–Strength Concrete; A testreport. 1992.
R 290. JENSEN, HENRIK ELGAARD: Creep and Shrinkage of High–Strength Concrete; A testreport; Appendix A. 1992.
R 291. JENSEN, HENRIK ELGAARD: Creep and Shrinkage of High–Strength Concrete; A testreport; Appendix B. 1992.
R 292. JENSEN, HENRIK ELGAARD: Creep and Shrinkage of High–Strength Concrete; A testreport; Appendix C. 1992.
R 293. JENSEN, HENRIK ELGAARD: Creep and Shrinkage of High–Strength Concrete; A testreport; Appendix D. 1992.
R 294. JENSEN, HENRIK ELGAARD: Creep and Shrinkage of High–Strength Concrete; An Analysis. 1992.
R 295. JENSEN, HENRIK ELGAARD: State–of–the–art Rapport for Revnet Betons Styrke. 1992.
R 296. IBSØ, JAN BEHRENDT & RASMUSSEN, LARS JUEL: Vridning af armerede normal– og højstyrkebetonbjælker. 1992.
R 297. RIBERHOLT, HILMER, JOHANNESEN, JOHANNES MORSING & RASMUSSEN, LARS JUEL: Rammehjørner med indlimede stålstænger i limtræ. 1992.

Abonnement 1.7.1992 – 30.6.1993 kr. 130,–
Subscription rate 1.7.1992 – 30.6.1993 D.Kr. 130.–.

Hvis De ikke allerede modtager Afdelingens resumeoversigt ved udgivelsen, kan Afdelingen tilbyde at tilsende næste års resumeoversigt, når den udgives, dersom De udfylder og returnerer nedenstående kupon.

Returneres til
Afdelingen for Bærende Konstruktioner
Danmarks tekniske Højskole
Bygning 118
2800 Lyngby

Fremtidig tilsendelse af resumeoversigter udbedes af
(bedes udfyldt med blokbogstaver):

Stilling og navn: .....

Adresse: .....

Postnr. og -distrikt: .....

The Department has pleasure in offering to send you a next year's list of summaries, free of charge. If you do not already receive it upon publication, kindly complete and return the coupon below.

To be returned to:
Department of Structural Engineering
Technical University of Denmark
Building 118
DK-2800 Lyngby, Denmark.

The undersigned wishes to receive the Department's
List of Summaries:
(Please complete in block letters)

Title and name .....

Address.....

Postal No. and district.....

Country.....